Department of Applied Physics

Study of Norway spruce cell wall structure with microscopy tools

Md. Mehedi Reza

Aalto University

DOCTORAL DISSERTATIONS

Aalto University publication series
DOCTORAL DISSERTATIONS 39/2016

Study of Norway spruce cell wall structure with microscopy tools

Md. Mehedi Reza

A doctoral dissertation completed for the degree of Doctor of Science (Technology) to be defended, with the permission of the Aalto University School of Science, at a public examination held at the lecture hall E (Otakaari 1, Otaniemi) of the school on 15 April 2016 at 12.

Aalto University
School of Science
Department of Applied Physics

Supervising professor
Professor Janne Ruokolainen

Thesis advisor
Professor Tapani Vuorinen

Preliminary examiners
Professor Junji Sugiyama
Kyoto University, Japan

Professor Ingo Burgert
ETH - Swiss Federal Institute of Technology
Zürich, Switzerland

Opponents
Professor Lennart Salmén
Innventia AB
Stockholm, Sweden

Aalto University publication series
DOCTORAL DISSERTATIONS 39/2016

ISBN 978-952-60-6683-7 (printed)
ISBN 978-952-60-6684-4 (pdf)
ISSN-L 1799-4934
ISSN 1799-4934 (printed)
ISSN 1799-4942 (pdf)
http://urn.fi/URN:ISBN:978-952-60-6684-4

Unigrafia Oy
Helsinki 2016

Finland

441 697
Printed matter

Aalto University

Abstract

Aalto University, P.O. Box 11000, FI-00076 Aalto www.aalto.fi

Author
Md. Mehedi Reza

Name of the doctoral dissertation
Study of Norway spruce cell wall structure with microscopy tools

Publisher School of Science

Unit Department of Applied Physics

Series Aalto University publication series DOCTORAL DISSERTATIONS 39/2016

Field of research Engineering Physics

Manuscript submitted 15 December 2015 **Date of the defence** 15 April 2016

Permission to publish granted (date) 2 February 2016 **Language** English

☐ **Monograph** ☒ **Article dissertation** ☐ **Essay dissertation**

Abstract

The distribution and orientation of wood cell wall polymers play an important role in its physical, chemical and mechanical properties, and thus in the transformation into final products. Specifically, the orientation of cellulose elementary fibrils (EF) controls the performance of wood in almost every end use. Moreover, lignin is covalently linked to many of the cell wall polysaccharides, which imposes a serious technical challenge during the degradation of cellulose into value added products. Therefore, the deep understanding of the organization of the cell wall materials is imperative.

In this study, normal Norway spruce wood was studied with a high-resolution cryo-transmission electron microscope (cryo-TEM). Both, two- (2D) and three-dimensional (3D) imaging techniques within TEM were applied on ultrathin wood sections to understand the wood structure. The defibration mechanisms in high-temperature thermomechanical pulping (HT-TMP) was also studied with a conventional TEM. Furthermore, the accessibility of cell wall lignin was studied with TEM and Raman microspectroscopy by analysing fresh and solvent extracted ultrathin sections of Norway spruce branch wood.

The results showed that the organization of EFs varies from layer to layer and also within a single layer. In addition to the well-adopted concept of longitudinal EF angle in tangential plane, this study showed the presence of an out-of-plane EF angle relative to the cell wall plane. The S_1 layer had a transverse EF orientation with a predominant radial lamellar structure of EF bundles. Both crossed and parallel EF orientations were detected in the $S_{1\text{-}2}$ transition layer, which was supported by the defibration mechanisms in HT-TMP. EFs in the outer-S_2 layer had a relatively high longitudinal EF angle and a large out-of-plane angle with respect to the tangential plane, which continued to decline inward and became almost axial in the inner-S_2 layer. A transverse, out-of-plane EF orientation in the S_3 transverse sections was observed. The models of the wood cell wall summarize most of the findings regarding the wood ultrastructure.

Study of the lignin extracted ultrathin sections showed the change of lignin concentration in all cell wall layers during the extraction process. However, lignin obtained after extraction consists mainly of secondary wall lignin as this area contains most of the total cell wall lignin in conifer tracheids.

The new observations on the wood cell wall structure may lead to a better understanding of the reactivity of cellulosic fibers in biochemical, chemical and mechanical treatments.

Keywords cellulose microfibril, lignin distribution, lignin extraction, Norway spruce, thermo-mechanical pulp, transmission electron microscopy, transmission electron tomography, Raman microscopy, ultrathin sectioning, wood cell wall

ISBN (printed) 978-952-60-6683-7 **ISBN (pdf)** 978-952-60-6684-4

ISSN-L 1799-4934 **ISSN (printed)** 1799-4934 **ISSN (pdf)** 1799-4942

Location of publisher Helsinki **Location of printing** Helsinki **Year** 2016

Pages 138 **urn** http://urn.fi/URN:ISBN:978-952-60-6684-4

Acknowledgements

I started this study in March 2011 when I joined Multidisciplinary Institute of Digitalization and Energy (MIDE) project. Although my official employment agreement was made with Department of Applied Physics, Aalto University, I was a doctoral student of School of Chemical Technology. In the beginning of 2014 my studentship was transferred to School of Science and Professor Janne Ruokolainen became official supervisor. While the MIDE project ended in June 2014, financial support for the research came from MolMat Graduate School of Department of Applied Physics. Funding for the last part of this study came from UltraWood Project funded by Academy of Finland.

First I want to thank my supervisor, Professor Janne Ruokolainen, for supervising this work and teaching me electron microscopy from the beginning. You made me a part of Nanomicroscopy Center and gave me the opportunity to learn electron microscopy. You taught me how to work independently.

I am very grateful to Professor Tapani Vuorinen, the thesis advisor, for choosing me to work in the MIDE project at the very beginning. You have guided me from the beginning of my study till the end. You accepted me to be a part of your research group, although I was belong to a different School. Thank you for everything you taught me throughout this journey. I really enjoyed every moment being a part of your research group.

I express my sincere gratitude to Dr. Anna-Stiina Jäskelainen for her encouraging speech and guidance before she had left the project, and Professor Eero Kontturi for his valuable instructions during my study. Thank you for being there for me!

I would like to thank Dr. Jani Seitsonen for teaching me the operations of transmission electron microscopes and Dr. Peter Engelhardt for teaching me electron tomography and 3D reconstruction. I am also thankful to Johannes Haataja for helping me to learn many software. I want to thank Joseph Campbell for proofreading my articles and dissertation. I also thank my co-authors for their valuable contribution.

A very warm thank to the ex- and current members of the Wood Chemistry Research Group. Special thanks go to Iina, Naveen, Emilia, Saija, Ghajaleh, Jinze, Leonardo, Carlo, Olesya, Akio, Andreas, Timo, Marcelo, Raili, Xiangmin. I further thank research colleagues and supporting staffs in Puu and Applied Physics. Special thanks go to Ahsan, Terho, Xiaqi, Alp, Pena, Hua, Lide, Nonappa, Arcot, Orvokki and Timo.

I would like to thank Bangladeshi community in Otaniemi. Special thanks go to Noman, Rony, Babu, Bulbul, Shyakh, Alam and Aftab for the friendship from the very first day in Finland.

I express my heartfelt gratitude for my parents, sisters, my wife and finally my lovely daughter Raima for your endless support, inspiration and sacrifices.

Last but foremost all the praise goes to almighty Creator for sending me to this Earth and giving me the opportunity to witness His fascinating creations.

Espoo, 22 February 2016

Md. Mehedi Reza

Contents

List of Publications

This doctoral dissertation consists of a summary of the following publications which are referred to in the text by their numerals

1. Reza, Mehedi; Kontturi, Eero; Jääskeläinen, Anna-Stiina; Vuorinen, Tapani; Ruokolainen, Janne. 2015. Transmission electron microscopy for wood and fiber analysis - A Review. BioResources, volume 10, issue 3, pages 6230-6261. ISSN 1930-2126.

2. Reza, Mehedi; Ruokolainen, Janne; Vuorinen, Tapani. 2014. Out-of-plane orientation of cellulose elementary fibrils on spruce tracheid wall based on imaging with high-resolution transmission electron microscopy. Planta, Volume 240, Issue 3, pages 565-573. ISSN 0032-0935. DOI 10.1007/s00425-014-2107-1.

3. Reza, Mehedi; Bertinetto, Carlo; Engelhardt, Peter; Ruokolainen, Janne; Vuorinen, Tapani. 2015. The ultrastructure of spruce S_1 and S_{1-2} layers based on high-resolution cryo-TEM tomography and computational modelling. (Submitted).

4. Solala, Iina; Antikainen, Toni; **Reza, Mehedi**; Johansson, Leena-Sisko; Hughes, Mark; Vuorinen, Tapani. 2014. Spruce fiber properties after high-temperature thermomechanical pulping (HT-TMP). Holzforschung. Volume 68, Issue 2, Pages 195-201. ISSN 0018-3830. DOI: 10.1515/hf-2013-0083.

5. Reza, Mehedi; Rojas, Leonardo G.; Kontturi, Eero; Vuorinen, Tapani; Ruokolainen, Janne. 2014. Accessibility of cell wall lignin in solvent extraction of ultrathin spruce wood sections. ACS Sustainable Chemistry and Engineering, Volume 2, Issue 4, pages 804–808. DOI 10.1021/sc400470m.

Author's Contribution

Publication 1: Transmission electron microscopy for wood and fiber analysis - A Review

Mehedi Reza wrote the first version of the manuscript and prepared the final version based on the co-authors' feedback.

Publication 2: Out‑of‑plane orientation of cellulose elementary fibrils on spruce tracheid wall based on imaging with high‑resolution transmission electron microscopy

Mehedi Reza prepared samples for transmission electron microscopy, took the micrographs, and analysed the micrographs. The author wrote the first version of the manuscript and prepared the final version based on the co-authors' feedback.

Publication 3: The ultrastructure of spruce S_1 and $S_{1\text{-}2}$ layers based on high-resolution cryo-TEM tomography and computational modelling.

Mehedi Reza prepared samples for transmission electron microscopy, took the micrographs and tilt-series, reconstructed the tilt-series, and built the schematic cell wall model. Computational analysis was performed by Dr. Carlo Bertinetto. The author wrote the first version of the manuscript and prepared the final version based on the co-authors' feedback.

Publication 4: Spruce fiber properties after high-temperature thermomechanical pulping (HT-TMP)

Mehedi Reza prepared samples for transmission electron microscopy, took the transmission electron micrographs, analysed the micrographs, and wrote the corresponding parts of the manuscript with co-authors.

Publication 5: Accessibility of cell wall lignin in solvent extraction of ultrathin spruce wood sections

Mehedi Reza performed lignin extraction, prepared samples for microscopy, took the micrographs and spectra, and analysed the micrographs and spectra. The author wrote the first version of the manuscript and prepared the final version based on the co-authors' feedback.

List of Abbreviations and Symbols

a.u.	arbitrary unit
EF	cellulose elementary fibril
EFB	elementary fibril bundle
C	cross/transverse section
CCML	cell corner middle lamellae
CesA	cellulose synthase complex
CML	compound middle lamellae
Cryo-TEM	cryo-transmission electron microscope
EW	earlywood
HT-TMP	high-temperature thermomechanical pulp
I_{CML}	Raman scattering intensity of lignin in the CML
I_{S2}	Raman scattering intensity of lignin in the S_2 layer
$I_{extracted\text{-}S2}$	Raman scattering intensity of lignin in the extracted S_2 layer
$I_{unextracted\text{-}S2}$	Raman scattering intensity of lignin in the unextracted S_2 layer
I_{1600}	scattering intensity at 1600 cm^{-1} Raman band
I_{1122}	scattering intensity at 1122 cm^{-1} Raman band
I_{α}	one of the polymorphs of cellulose
I_{β}	one of the polymorphs of cellulose
$KMnO_4$	potassium permanganate
L	lumen, longitudinal axis
LW	latewood
MFA	microfibril angle
ML	middle lamellae
MnO_2	manganese dioxide
OsO_4	osmium tetroxide

P	primary wall
R	rays, radial plane/surface/section
RC	resin canal
RM	Raman microspectroscopy
ROI	region of interest
SEM	scanning electron microscopy
S-helix	left-handed helical orientation
SIRT	simultaneous iterative reconstruction technique
S_1	outermost layer of the secondary wall
S_2	middle layer of the secondary wall
S_{1-2}	transition layer between S_1 and S_2
S_3	innermost layer of the secondary wall
T	tangential plane/surface/section
TEM	transmission electron microscopy
W	warty layer
Z-helix	right-handed helical orientation

1. Introduction

The composition of wood cell walls plays an important role in its physical, chemical and mechanical properties, and thus, in the transformation of wood into final products. Being surrounded by a matrix of lignin and hemicelluloses, cellulose elementary fibrils,[1] also known as microfibrils,[2] form the semicrystalline skeleton of the wood cell wall.[3,4] The smallest cellulosic strand will herein, for simplicity, be referred to as elementary fibril (EF). In addition to the supramolecular arrangement of the cell wall polymers, lignin is covalently linked to many of the cell wall polysaccharides, thus strengthening the fiber structure. The tight arrangement of the cell wall components always imposes a serious technical challenge during the degradation of cellulose into glucose for the production of biofuels, and during the dissolution of pulps in order to regenerate textile fibers. In the preparation of cellulose nanofibrils, fibers are treated with chemicals and/or enzymes in order to open up the fibrillar network of the wood cell wall during a subsequent mechanical disintegration. However, the EF aggregates that exist in wood and pulp reduce the accessibility of cellulose and hamper the action of enzymes and chemicals.[5] Despite extensive research on wood cell wall structure, the detailed distribution and organization of cell wall components is still far from being fully understood. The most apparent reason for the deficiency of knowledge is the insufficient resolution of the methods used in existing studies and hindrances in sample preparation.

According to the literature, EFs are helically oriented in concentric planes of wood cells. The presence of EF structures (*e.g.* lamellae, aggregates, bundles) in the S_2 layer of softwood tracheid was reported in several studies.[6-10] However, the organization (radial/tangential) of these structures has been an unsettled topic.[7,11] The orientation of EFs in the transition layers of the secondary wall is also poorly understood. The principal limitation of the studies on which current cell wall models are based is that most of them employed conventional low resolution imaging techniques[12] and were done mainly on the transverse section of the thick S_2 layer.

1.1 Outline of the thesis

The main objective of this thesis was to investigate the orientation of elementary fibril (EF) structures in the wood cell wall. Two- and three-dimensional imaging techniques within transmission electron microscopy (TEM) were ap-

plied on ultrathin spruce sections to obtain high-resolution information on the EF structures. Spruce thermomechanical pulp (TMP) sections were studied with a TEM to observe the defibration mechanism during the mechanical processing of wood. Furthermore, ultrathin sections of spruce branch wood were studied with Raman microspectroscopy and TEM before and after extracting lignin with 1,4-dioxane to trace the progress of lignin extraction.

This dissertation consists of five publications exploring the high-resolution structure of wood cell walls. **Figure 1** summarizes the outline of the thesis. **Publication 1** is a review article summarizing the application of TEM in wood and fiber analysis. **Publication 2** includes the high-resolution transmission electron micrographs, and a wood cell wall model showing the EF orientation in the tracheid secondary wall. **Publication 3** comprises follow-up research of Publication 2 where three-dimensional electron tomograms of the wood cell wall visualizing the orientation of EF structures in the S_1 and S_{1-2} layer have been presented and finally, added to the cell wall model. **Publication 4** includes TEM images of TMP showing the defibration mechanism of pulp fibers during the mechanical processing of wood. **Publication 5** includes Raman micrographs and spectra, and TEM images of lignin extracted, ultrathin sections of branch wood. The progress of lignin extraction and the distribution of residual lignin in the cell wall were studied and described in this paper.

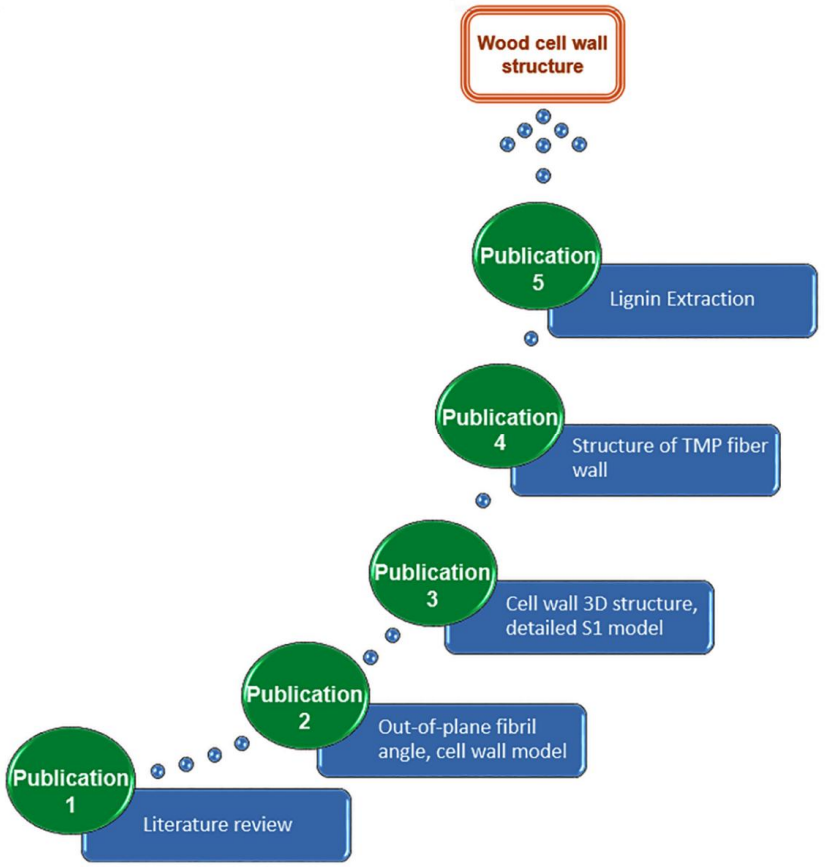

Figure 1. Thesis outline; TMP, thermomechanical pulp.

2. Background

2.1 Wood structure

All seed-bearing tree species are divided into gymnosperms and angiosperms. Conifers, *i.e.*, softwood species (*e.g.*, Norway spruce) are gymnosperms and broad-leaved, *i.e.*, hardwood species (*e.g.*, birch) are angiosperms. In trees, the secondary growth is formed by a thin layer of living cells called the vascular cambium (**Figure 2**) that, by repeated cell divisions, produces phloem cells (or bark) on the outside and secondary xylem (or wood) on the inside. The functioning of cambium responds to the alternation of seasons from cold to warm or dry to rainy. Tropical plants exhibit cambial activity throughout the year, whereas temperate zone plants have only one growing season and the rest of the year remains dormant.[13] Wood formed during the summer, *i.e.*, latewood, provides mechanical strength to the tree while earlywood is mainly responsible for water and mineral conduction. The lateral transport of liquids occurs through the natural openings in the cell walls called pits. The xylem is normally divided into sapwood and heartwood; the former contains both living and dead cells and the latter is comprised entirely of dead cells. The heartwood is less permeable and more durable because of the formation and deposition of phenolic compounds and other extractives. The xylem formed within a single growing season is normally organized into a distinct concentric ring, which is referred to as the annual growth ring.

Softwood consists of a limited number of different cell types and is more or less uniform and simple compared to hardwood. Softwood xylem is mainly composed of longitudinal tracheids (90 - 95 %). In Norway spruce, tracheids comprise over 90 % of the total cell volume.[14] Softwood xylem also has a smaller amount of ray parenchyma (5 - 10 %), ray tracheids and epithelial cells surrounding resin canals.[3,15] **Table 1** shows the average diameter and thickness of tracheids in spruce earlywood and latewood. In Norway spruce, the average length of tracheids is 3.4 mm.[3] Tracheids have a hollow centre (*i.e.*, lumen) and closed ends. The major functions of the tracheids are to provide mechanical support (latewood) and to conduct water and minerals (earlywood).

Table 1. Wall thickness and diameter of earlywood and latewood tracheids in Norway spruce.[14]

Properties		Earlywood	Latewood
Tracheid wall thickness (µm)	Radial	3.52	6.23
	Tangential	2.90	4.69
Tracheid diameter (µm)	Radial	39.30	13.10
	Tangential	32.70	32.10

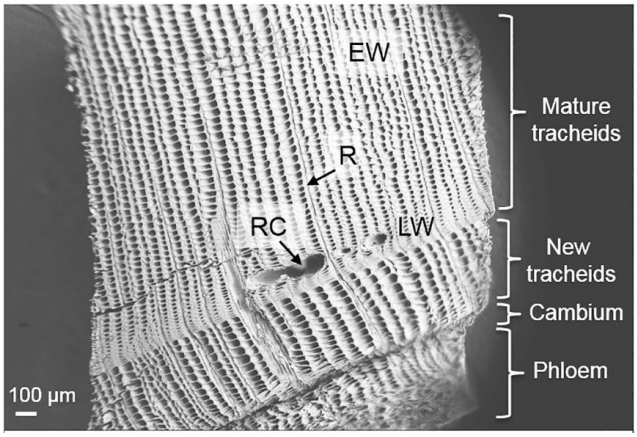

Figure 2. An SEM image of a Norway spruce transverse section through xylem and phloem. EW, earlywood; LW, latewood; R, rays; RC, resin canal.

2.2 The wood cell wall

Wood is a structured material with different levels (length scales) of hierarchy that might be termed as the integral (tree), macroscopic (annual rings), microscopic (wood cells), ultrastructural (cell wall), nanostructure (EF structures) and molecular (polymers) characteristics (**Figure 3a**).[16] The cell wall of wood is built up of several layers and sublayers, namely, the middle lamellae (ML), the primary wall (P), several sublayers of secondary wall (S_1, S_2 and S_3) and an additional warty layer (W).[17] Since the ML is quite difficult to distinguish from P, ML and the two adjacent Ps are normally referred to as a compound middle lamella (CML). The average shares of the CML, S_1, S_2 and S_3 of the whole softwood tracheid wall were reported to be 4.2, 12.5, 78.7 and 4.5 % in earlywood; and 2.1, 9, 85.4 and 3.3 % in latewood, respectively.[3] High variability in the thickness of the different layers of the wood cell wall was reported in several different investigations.[18,19] There are quite many models of the wood cell wall available in the literature depicting the average distribution and orientation of cell wall materials based on different imaging techniques (**Figure 3b**); however, the true structure of the cell wall is still controversial.[4,11,17,20,21] Many exceptions from these models are reported in the literature.[3,17] Electron micrographs of the wood cell wall of *Fraxinus mandshurica* also showed two layers (S_1 and S_2) in the secondary wall.[22] Although it is well known that the orientation and distribution of cell wall materials vary to a large extent within the tree, this is seldom considered in the models. The layering of the wood cell wall can be observed with a conventional light microscope, but the clear structural differences can only be seen with electron microscopes.

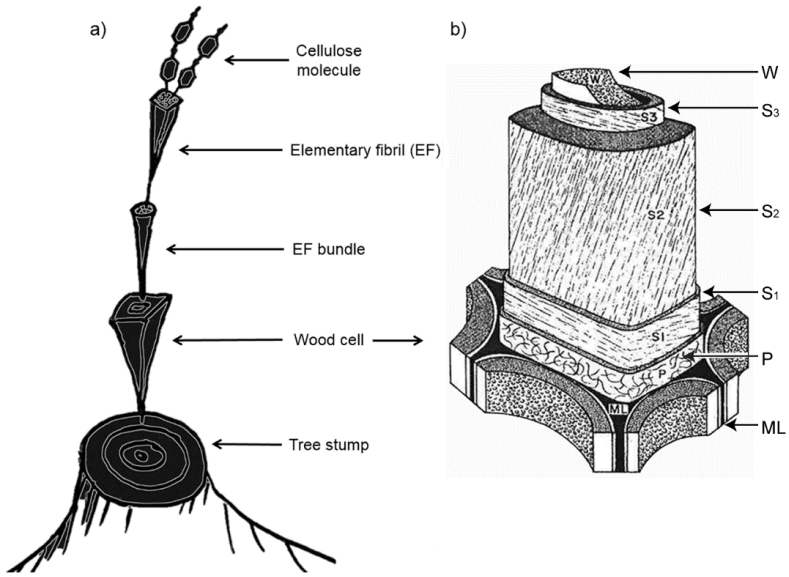

Figure 3. (a) A schematic diagram of wood depicting the hierarchical structure (from macroscopic to molecular); and (b) an accepted model of the wood cell showing the average fibril orientation in different layers (Figure republished from Côté 1967)[23]. W, warty layer; S_1, S_2, S_3, layers of the secondary wall; P, primary layer; ML, middle lamellae.

2.3 Structure and orientation of elementary fibrils

The fibrillar structure of cellulose was confirmed a long time ago in electron micrographs of plant materials.[24,25] Micrographs suggest that elementary fibrils (EF) are synthesised in the plasma membrane by cellulose synthases (CesA) consisting of a ring of six particles, called a "rosette".[26,27] Correlation between the CesA alignment in the plasma membrane and the cortical microtubules has been reported in several studies.[28] Following deposition, the orientation of EFs gradually changes until the termination of cell expansion.[29] EFs are about 3.5 nm wide[4,30] and are regularly connected with a bridging element[31]. Electron diffraction on native cellulose from the algal cell wall showed the coexistence of both I_α and I_β crystal structures with variable proportions.[32,33] Models of EFs consisting of 36 (**Figure 4a**) and 24 cellulose chains were proposed using different analytical techniques,[34-36] where crystalline chains are surrounded by less-crystalline and amorphic chains. Furthermore, the crystalline structure is repeatedly interrupted by disordered cellulose chains along the fibrils (**Figure 4b**).[37] The arrangement of crystalline and disordered cellulose is not well understood, but 4 - 5 misaligned units every 150 nm were reported in the case of ramie fibers.[38] Since surrounding matrix material affects the analysis,[39] EFs in a matrix with fewer noncellulosic polymers are often preferred, such as cotton that also has much bigger crystal dimensions. These models are speculations of the true structure of EFs in the native wood cell wall.

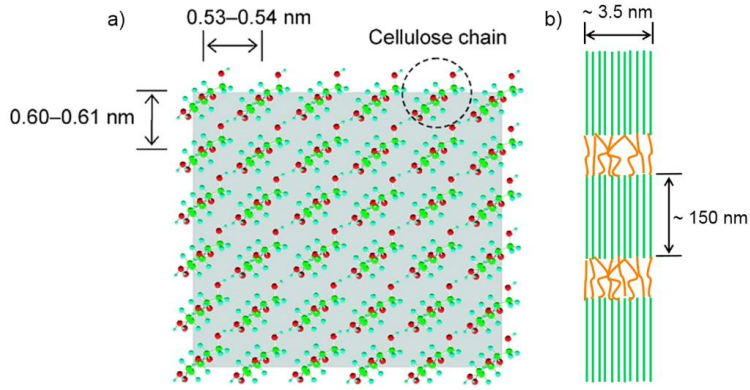

Figure 4. Schematic models of elementary fibrils: (a) cross section with 36 cellulose chains (Reprinted with permission from Okita et al.[40]. Copyright 2010 American Chemical Society); (b) arrangement of crystalline (green) and amorphous (orange) regions along the fibril.

EFs in electron micrographs appear as series of interconnected granular particles.[41,42] The aggregation of cellulose elementary fibrils in wood and pulps was reported in several investigations.[24,41,43,44] These aggregates appear as bundles in the micrographs of the transverse section of the tracheid S_2 layer.[6,45] A model depicting the arrangement of EFs in bundles is presented in **Figure 5a**. The aggregation of EFs in wood and pulps controls the accessibility of cellulose,[46] and thus affects the extraction of cell wall components in biorefinery processes. There are quite many terminologies (*e.g.* bundles, radial agglomerations, aggregates, macrofibrils, *etc.*) used in the literature to label the EF structures in the wood cell wall.[6,9,10,45] Often, different terms are used to explain the size differences between the EF structures. The arrangement of EF aggregates in the secondary wall has been an unresolved topic.

A radial arrangement of EF structures was observed on the transverse fracture surfaces of wood,[11] whereas Fahlén and Salmén[7] suggested that the radial patterns on the fracture surfaces are the result of energy release during fracturing. There are also numerous papers that reported a tangential pattern for normal wood. Donaldson[10] observed a predominantly random arrangement of aggregates in a high-resolution SEM study, but occasionally they may show either the tangential or radial patterns. It should be mentioned that the previous studies were mainly conducted on the S_2 layer and using 2D imaging techniques.

The orientation of EFs in different cell wall layers varies. The helical organization of EFs has frequently been depicted in models of wood cell wall.[17,47] The angle between the tracheid axis and EFs is called the microfibril angle (MFA) and the helix of fibrils is symbolized either as S for left-handed helices or Z for right-handed helices.[48] In particular, the S_1 layer has transversely oriented EFs, the thick S_2 layer has axially oriented EFs and the S_3 layer has transversely oriented EFs, in an S-Z-S helical organization (**Figure 3b**).[48-51] In the tracheid S_1 layer both S- and Z-helical orientations with an impression of crossed-fibrillar structure was reported;[20,52] however, EFs more or less perpendicular with respect to the fiber longitudinal axis were observed in a single helix in

recent studies.[44,48,49] The general consensus is that the tracheid S_2 layer consists of several concentric lamellae (**Figure 5b**),[4,53] which had been, however, interpreted as tangential striations by Chafe.[54]

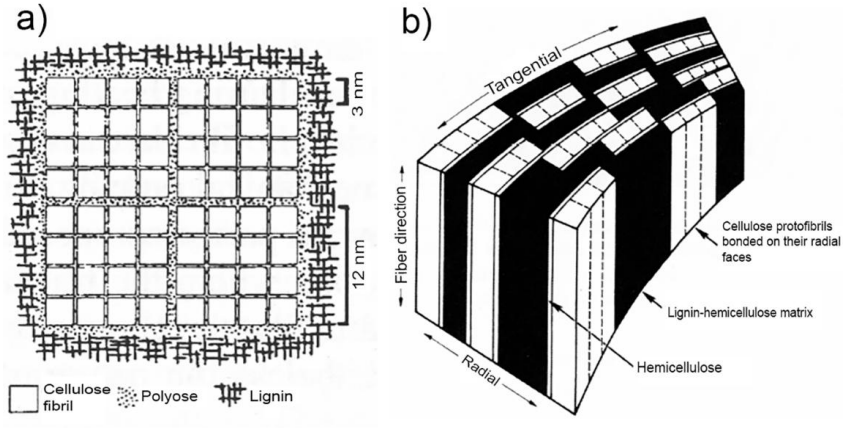

Figure 5. Models showing the arrangement of wood polymers in the cell wall. a) Fengel and Wegener[55] proposed a model with elementary fibrils surrounded by monolayer of hemicellulose and larger units (bundles) surrounded with a matrix of lignin/hemicellulose; and b) Model illustrating cellulose fibrils forming interrupted lamellae embedded in a lignin/hemicellulose matrix (from Kerr and Goring[4]).

An abrupt change in the EF orientation between the S_1 and the S_2 layers in Norway spruce was reported in several studies,[44,49] whereas no clear transition was observed between the S_2 and the S_3 layers.[50] An intermediate structure between the layers in the secondary wall was suggested by Wardrop.[56] The orientation of EF bundles in the secondary wall was studied with an SEM from the lumen side; however, the transition between the layers could not be traced due to the progressive change of EF orientation.[51,57] Brändström and colleagues[49] consider the transition between S_1 and S_2 as a part of the S_2 layer. Due to the tight EF arrangement, the transition layers are known as sheets of high cellulose content.[58]

2.4 Lignin distribution

Lignin is a major cell wall component contributing to the mechanical strength of wood fibers as well as contributing to the water proofing function of conductive cells. Lignin is aromatic and branched polymer which holds phenolic and non-phenolic units. It has three main phenolic precursors or monolignols (**Figure 6**): *p*-coumaryl, coniferyl and sinapyl alcohols, which are all products of the plant phenylpropanoid pathway.[59] Softwood lignin, also known as guaiacyl lignin, mainly consists of coniferyl alcohol and may contain a small amount of *p*-coumaryl alcohol, particularly in compression wood, whereas hardwood lignin consists of both coniferyl and sinapyl alcohols. Small amount of *p*-coumaryl alcohol is also perhaps present in hardwood lignin.[60]

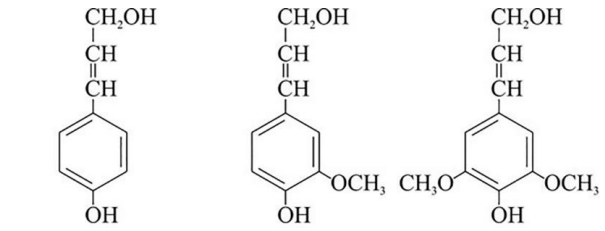

Figure 6. The principal monolignols forming the lignin polymer.

The structure of the developing, unlignified middle lamella in the cambium/developing xylem is a fine network, probably containing pectin and hemicelluloses.[61,62] As lignification proceeds, the middle lamella (ML) becomes compact, dense and partly covered with globular structures.[61] The ML region of wood cells is rich in lignin that glues adjacent wood cells together. However, because the secondary wall shares a much greater volume than the comparatively thin ML, most of the cell wall lignin is present in the secondary wall.[63] The cell corner middle lamella is often reported to be more highly lignified than other parts of the ML.[64] A heterogeneous lignin distribution in the ML attached to the thermomechanical pulp fibers of rubber wood was reported.[65] Studies supporting both homogeneous and inhomogeneous lignin distribution in the tracheid S_2 layer are available.[6,8,66,67]

2.5 Thermomechanical pulping

Thermomechanical pulping (TMP) is the dominant process for production of mechanical pulps in which fibers are separated, where moist wood chips are mechanically refined at elevated temperature (*ca.* 120 °C) and pressure. In commercial TMP mills, wood chips pass through a narrow gap of grooved metal discs so that the chips are broken down to fibers and other fragments. The downside of mechanical pulping is its high energy consumption. Increasing the temperature in TMP preparation, however, lowers the specific energy consumption by softening the wood structure, but results in fiber shortening.[68-70] Pulps produced by TMP are traditionally used in newsprint for its good optical properties and high yield. TMP fibers have a high lignin content (*ca.* 30 %), which makes them prone to yellowing upon exposure to light and moisture.

2.6 Transmission electron microscopy of wood specimens

2.6.1 Principle of image formation in TEM

In TEM, an energized beam of electrons are emitted from the electron gun, which then passes through the ultrathin specimen and exciting the fluorescent screen/detector to image the sample. The electron beam allows higher resolving power than visible light in optical microscopy because the wavelength of an electron is very short. Generally, in electron microscope primary electron

beam hits the specimen and is transformed into a non-uniform electron intensity after transmission or scattering by the specimen. This non-uniform electron intensity translates into image contrast on the screen after hitting the electron detector. Either the direct beam or a diffracted beam is used to form bright- and dark-field images respectively. A full description of image formation in TEM can be found in Williams' and Carter's textbook.[71] **Figure 7** illustrates the mechanism of image formation in bright-field imaging mode in a TEM. An objective aperture is used to block scattered electrons in bright-field mode in order to enhance the contrast. Contrast can be enhanced further by using an energy filter to remove inelastically scattered electrons. Moreover, while interacting with the specimen, a range of secondary signals are produced. Many of them are used in analytical electron microscopy, giving clues to the chemical composition and other information about the specimens. An ultra-high vacuum column is necessary to prevent scattering of the electron beam by ambient gas molecules.

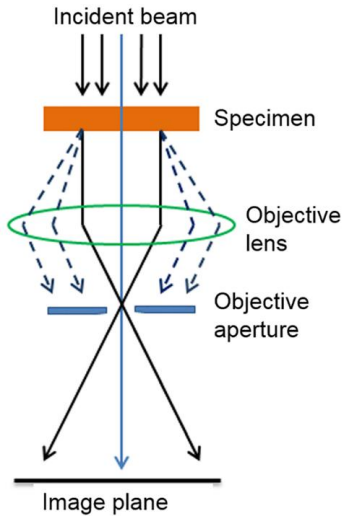

Figure 7. Image formation in a TEM in bright-field imaging mode using the direct beam (solid lines). Dashed lines show scattered electrons. Figure republished from Reza *et al.*[72] (Publication 1).

2.7 Imaging of wood specimens with TEM

Because of the extraneous materials, low crystallinity, and tight association of cell wall polymers, it has always been challenging to image the structure and morphology of the wood cell wall. Wood specimens are also more susceptible to radiation damage than the highly crystalline *Valonia*. The radiation damage caused by the electron beam can be reduced to an extent by using a higher accelerating voltage.[72] The nonlignified/less-lignified gelatinous layer in tension wood fibers was also found to be a suitable specimen to image with the direct beam.[73] The development of cryo-TEM also provided the opportunity to image beam-sensitive specimens with a substantial electron dose. In cryo-TEM, the specimen temperature is kept below 20 K using liquid helium during imaging.

This way, the electron dose can be increased at least ten times compared to room temperature.[73]

2.8 Transmission electron tomography

Electron tomography is a useful technique for revealing 3D information about wood structure since TEM micrographs provide only 2D projections of the 3D objects. In tomography, a series of images are taken at different tilt intervals and reconstructed into a 3D volume. X-rays also can be used for tomography, and has been applied to spruce wood; however, researchers were only able to observe the features with dimensions over 1.5 μm.[74] In contrast, TEM, having an electron beam with shorter wavelength, is capable of acquiring a tilt series from +60° to -60° at angular increments of about 1° to 3°, thus generating high-resolution (nm scale) electron tomograms after the reconstruction (**Figure 8**). Electron tomography has been used for over 30 years and has been a useful technique for exploring 3D biological structures. However, the sample may suffer from beam damage during data acquisition because the sample is continuously exposed to the electron beam during the generation of a tilt series. This problem can be overcome, to an extent, by using cryo-TEM and the low-dose mode of automated acquisition software.

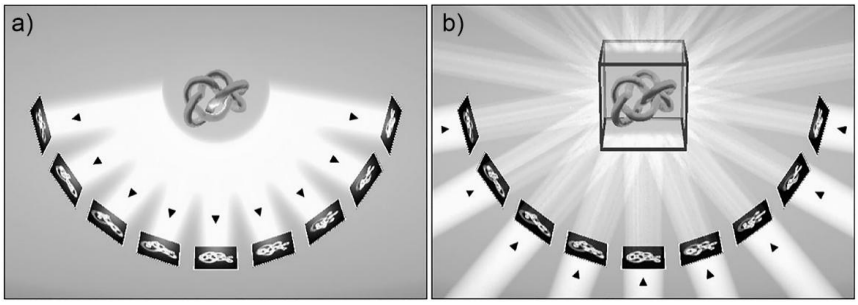

Figure 8. Schematic representation of electron tomography. a) A set of projections of a flexible rope knot (object) is recorded on a camera while the object is tilted incrementally around an axis perpendicular to the electron beam. b) The back-projection method explains the principle of the 3D reconstruction. For each projection, a back-projection body is calculated, and the sum of all projection bodies yields the density distribution of the original object — the tomogram.[75]

Further image processing might be necessary to separate individual EFs digitally in the tomograms.[76] Xu and colleagues[9] performed dual-axis electron tomography to investigate the 3D organization of cellulose EFs in plastic resin-embedded, delignified cell walls of radiata pine early wood. Xu *et al.* were able to digitally isolate individual EFs from associated lignin and hemicelluloses (**Figure 9**) by a user driven segmentation method – they stained the wood sections with several chemicals to enhance contrast and beam stability.

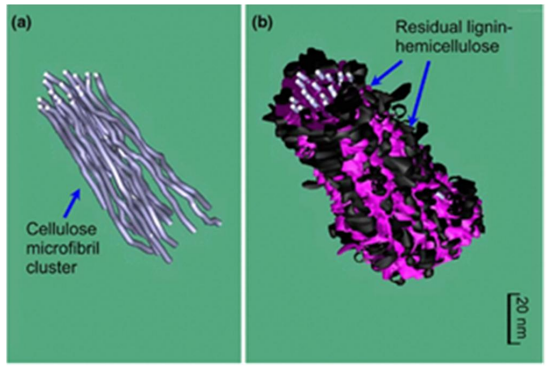

Figure 9. Models of an elementary fibril cluster (EF) in the radiata pine S_2 layer obtained by tracking tomographic slices. (a) An EF cluster without associated matrix materials; and (b) model of the same cluster with residual lignin and hemicelluloses. Figure republished from Xu *et al.*[9] with permission given by Springer-Verlag.

2.8.1 Sample preparation

Preparing ultrathin sections

For TEM analysis, specimens must be ultrathin so that electrons can transmit through it. For sectioning, an ultra-microtome equipped with a diamond knife or a glass knife is usually used (**Figure 10**). Before sectioning, samples are normally embedded in resin to resist deformation.[77,78] There are many advantages of embedding in resin, such as to preserve the fine structures, to aid in sectioning, and to reduce drifting in TEM. Resin embedded samples are sectioned in distilled water to get flat straight sections.

Cryo-sectioning of hydrated samples followed by cryo-TEM helps to avoid chemical fixation and structural changes due to dehydration. Sectioning also depends on the features of the sample under investigation.[50] Oblique sectioning has been performed to expose a large EF surface to enzymes.[79]

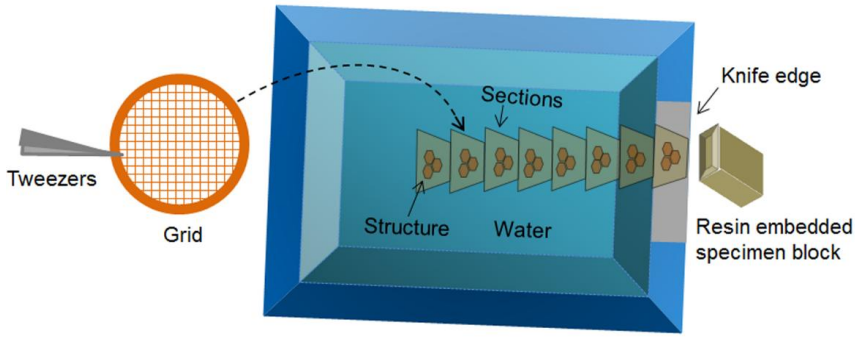

Figure 10. Schematic diagram of sectioning of a resin embedded specimen. Ultrathin sections are floating on the distilled water surface and are picked onto the TEM grid by gently touching the sections (Publication 1).[72]

Staining of wood specimen

Staining is an important step in specimen preparation for TEM. Polymeric samples like wood are mainly composed of light elements such as C, H, N and

O. The difference in electron density between these elements is not usually sufficient to form enough image contrast in TEM. Therefore, an auxiliary technique is needed to increase contrast differences between the structures under investigation. Staining is done by depositing high-density metal compounds to be adsorbed and absorbed by the specimen. Staining with heavy elements will also increase the specimen stability in the microscope. Potassium permanganate ($KMnO_4$), osmium tetroxide (OsO_4) and uranyl acetate are the frequently used stains for wood analysis with TEM.

$KMnO_4$ is a broadly used stain to contrast lignin in wood sections,[77] although there are suggestions that it may also stain some hemicelluloses but not cellulose.[80] Investigations on lignin model compounds showed that phenols, especially di- and triphenols, rapidly reduce permanganate to manganese oxides (MnO_2).[77] Finally, the resulting MnO_2 is deposited on the section showing the reaction sites.[81] According to the degree of lignification, the different cell wall layers show notable differences in their contrast and can be viewed with TEM.[82] The staining time can vary from 2 minutes to 2 hours.[77,83] In some cases pre-staining of wood blocks is preferred,[8,84] as post-staining can result in contamination of sections with MnO_2.[78]

Osmium tetroxide (OsO_4) is a strong oxidizing agent that oxidizes many organic materials and is itself reduced to elemental osmium, an easily visible black substance. OsO_4 does not stain carbohydrates (cellulose).[85] Thus, the dark contrast regions that appear in the electron micrographs of OsO_4 stained wood cell walls originate from lignin or its precursors.[86] OsO_4 reacts with double bonds and with di- and trihydroxy phenols.[77] However, compared with $KMnO_4$, OsO_4 only slightly stained *Pinus radiata* wood sections in the middle lamella region.[77]

Uranyl acetate has been a widely used negative stain. The main reason for negative staining is to surround the object in a suitable electron dense material, which provides high contrast and good preservation. Uranyl acetate has been mainly used for studying nanocellulose[87] and fines in suspension[88].

The combination of different staining methods has been applied to enhance the contrast and stability of wood specimens in TEM. Fernando and Daniel[89] used OsO_4 and ruthenium red as pre-staining chemicals followed by post-staining with $KMnO_4$ to study the lignin distribution in the cell wall of pine and spruce TMP shives. OsO_4 has also been used as a pre-staining chemical prior to post-staining with lead citrate to study the ultrastructure of wood.[90]

2.9 Raman microspectroscopy

Raman microspectroscopy (RM) is a vibrational spectroscopic technique that provides information about chemical composition of materials based on the analysis of the inelastic scattering of the light interacting with the induced electric dipole of chemical bonds (**Figure 11**). The frequency shift observed between the incident and scattered light is assigned to a particular vibration mode of a chemical bond. Moreover, RM allows high resolution mapping (0.6 – 1 μm) in a non-destructive manner. RM analysis has allowed the evaluation

of polymer distribution[58,66,91,92] and orientation[93-95] in the plant cell wall. Raman spectra of model compounds have been measured to detect their applicability in studying lignocellulosic materials.[96-100] RM is a valuable asset because of its ability to yield simultaneous chemical and morphological information of the plant cell wall.

First an area of interest is chosen using an optical microscope. Then, Raman spectra are collected within the area at regular intervals. The sample needs to be in focus of the microscope during the entire mapping. Subsequently the baselines of the spectra are corrected and characteristic bands representing the features of interests are chosen. Raman images are constructed by integrating characteristic Raman bands from the corrected spectra.

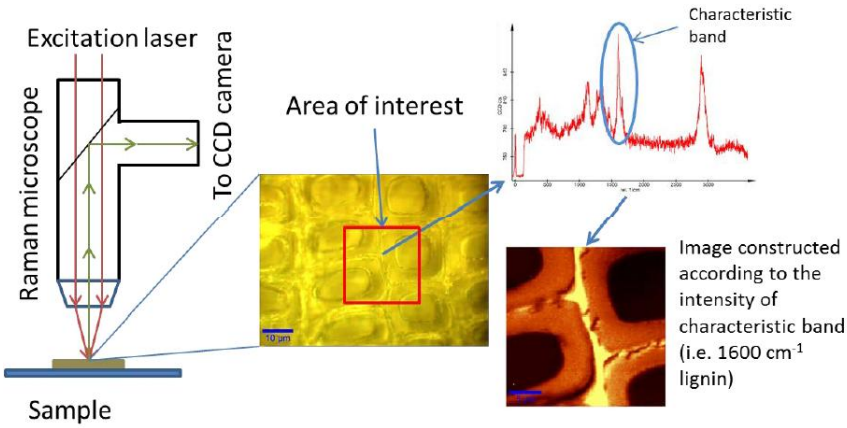

Figure 11. Schematic diagram of a Raman microscope and the basic principle of imaging.[101]

3. Materials and Methods

3.1.1 Materials

A diagram summarizing the experimental methods is presented in **Figure 12**.

For studying wood ultrastructure (**Publications 2 and 3**), a disk of wood was collected from breast height (~ 1.3 m) of a ~ 40-year-old Norway spruce (*Picea abies*) tree originating from Ruotsinkylä in Southern Finland. Cubes representing both earlywood and latewood were prepared before sectioning.

For the lignin extraction experiment (P**ublication 5**), a portion of Norway spruce branch wood was collected from Otaniemi, Espoo, Finland.

Thermomechanical pulp (TMP) samples were prepared from Norway spruce chips provided by the UPM Jämsänkoski mill. Mechanical pulping was performed in a wing defibrator (Defibrator Ab, Stockholm). A full description of the method can be found in Muguet *et al.*[102] Refining temperatures of 130 °C, 140 °C, 150 °C, 160 °C, or 170 °C were applied for approximately 2 or 5 min (**Publication 4**).

1,4-dioxane for lignin extraction and $KMnO_4$ for staining were used as received from Sigma-Aldrich.

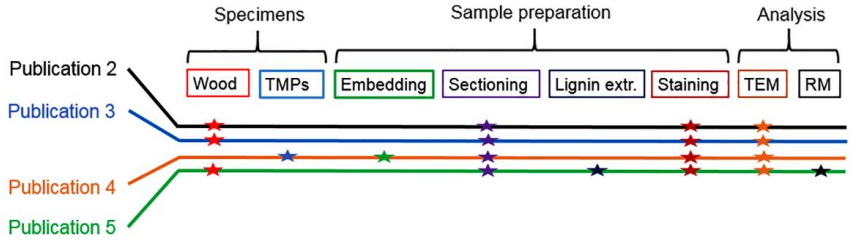

Figure 12. Schematic diagram showing the materials and methods for this study. TMP, thermomechanical pulp; extr., extraction; TEM, transmission electron microscopy; RM, Raman microspectroscopy.

3.1.2 Sectioning

For studying wood ultrastructure (**Publications 2 and 3**) and lignin extraction (P**ublication 5**), cubes ($3 \times 5 \times 10$ mm^3) of wood were prepared without embedding them in resin before sectioning. None of the cubes contained pith or cambium cells. The cubes were trimmed with a diamond knife followed by making trapezoids on the faces of the cubes where sectioning would be performed. Ultrathin sections (~ 50 - 200 nm) from different wood surfaces

(**Figure 13**) were cut with a diamond knife at room or cryogenic (−40 °C) temperature using a Leica EM FC7 ultra-microtome. The sections (50 – 150 nm thick) of stem wood for studying ultrastructure were collected on Cu grids with lacey carbon films, whereas sections (~ 200 nm thick) of branch wood for lignin extraction experiment were collected on 300 mesh hexagonal copper grids without any support film. Radial and tangential sections for studying wood ultrastructure were assumed to predominantly contain tangential and radial walls respectively.

TMP samples were embedded in epoxy resin (Vachticon, Hamburg) before sectioning in **Publication 4**. Ultrathin transverse sections of about 200 nm were cut in distilled water at room temperature with a diamond knife on the Leica EM FC7 ultra-microtome. The sections were collected on 600 mesh hexagonal Cu grids.

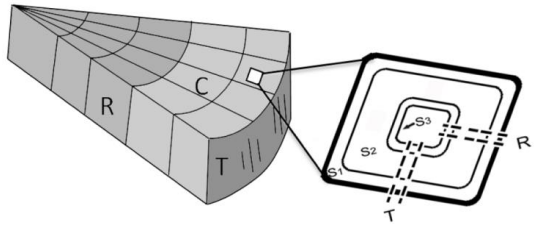

Figure 13. Schematic illustration of wood planes and the locations of wood sections. R, radial section; T, tangential section; C, cross/transverse section (Publication 2).

3.1.3 Lignin extraction (Publication 5)

For lignin extraction ~ 200 nm thick branch wood sections were placed in Petri dishes filled with 1,4-dioxane. After 1 hour, the grids were removed and gently washed with pure 1,4-dioxane. The short extraction time was considered to be sufficient because of the ultrathin sections.

3.1.4 Staining

Sections of wood for studying ultrastructure (**Publications 2 and 3**) with TEM were post-stained (after sectioning) with 1 % $KMnO_4$ for 25 – 30 min. $KMnO_4$ is a stain specific for lignin that improves contrast in lignin rich regions of the wood cell wall.[77] Sections of branch wood, both unextracted and extracted, for studying lignin extraction (**Publication 5**) were stained with 1 % $KMnO_4$ for 30 min. Resin embedded TMP (**Publication 4**) sections were post-stained for 1 hour with 1 % $KMnO_4$. All the sections were washed with distilled water after staining and subsequently dried before imaging with TEM.

3.1.5 Transmission electron microscopy

The ultrathin wood sections for studying wood ultrastructure were studied with a cryo-TEM (Jeol JEM-3200FSC) at an accelerating voltage of 300 kV. Micrographs were recorded using the Gatan Ultrascan 4000 CCD camera. The imaging was performed using zero loss energy filtering (Omega type) with a

slit width of 20 eV. Specimen temperature was maintained at −187 °C with liquid N_2 or −255 °C with liquid He during imaging (**Publications 2 and 3**).

Sections of branch wood and TMP samples were investigated with an FEI Tecnai 12 TEM at 80 or 120 kV at room temperature (**Publications 4 and 5**).

All the images were captured in bright-field imaging mode using Gatan DigitalMicrograph software.

3.1.6 Electron tomography (Publication 3)

Acquiring tilt series

Single-axis tilt series of transverse and radial longitudinal wood sections (**Figure 13**) were acquired by tilting the specimens from -60° to +66° at 3° angular increments using SerialEM software[103] at a pixel size of ~ 0.45 nm (unbinned) or ~ 0.9 nm (binned 2x). Micrographs were recorded with the Gatan Ultrascan 4000 CCD camera on the cryo-TEM (Jeol JEM-3200FSC) at an accelerating voltage of 300 kV. The images were taken in bright-field mode and using zero loss energy filtering (Omega type) with a slit width of 20 eV. The low-dose mode of the acquisition software was used during the data collection. Specimen temperature was maintained at −187 °C during imaging.

Tomogram assembly and visualisation

Tilt series were aligned by tracking 25 - 35 gold markers (~ 15 nm) with the IMOD software package.[104] Tomograms were reconstructed from the tilt series using the Simultaneous Iterative Reconstruction Technique (SIRT) within IMOD using 10 iterations. Finally, tomographic volumes were visualized with volume viewer plugin of ImageJ.[105] Gaussian filtering within UCSF Chimera was applied to reduce the noise to some extent.[106] In order to avoid effect of sectioning on wood structure,[107] images were mainly captured from the middle part of the tomograms.

Computational modelling

Tomographic subvolumes were imported and displayed in Matlab R2015a (The Mathworks, USA) using functions adapted from the PEET software package.[76] Thirty one and thirteen subvolumes were selected for the S_1 layer with fibrous structures and $S_{1\text{-}2}$ transition layer, respectively. In order to verify the consistency of results, several of these subvolumes were overlapping. They were rotated to approximately align the EFs with one of the axes or, in the case of the $S_{1\text{-}2}$ transition layer, with the bisector between two axes. The minimization of the cost function was performed initially using a Particle Swarm Optimizer[108] and then refined by the simplex method with the Matlab function 'fminsearch'.

3.1.7 Building the cell wall model (Publications 2 and 3)

The schematic 3D model of wood cell wall was built with Blender software (v2.68).[109]

3.1.8 Raman microspectroscopy (Publication 5)

Raman microspectroscopy was used to study the progress of lignin extraction from the ultrathin wood sections with 1,4-dioxane. The sections (~ 200 nm) of branch wood were examined with an alpha300 R confocal Raman microscope (Witec GmbH, Germany) equipped with a piezo electric scanner at ambient conditions. A frequency doubled Nd:YAG laser (532 nm, 10 mW) was focused onto the sample using a 100× (Nikon, NA = 0.95) air objective. The excitation laser was horizontally polarized. The spectra were acquired using a CCD (DU970N-BV) behind a grating (600 grooves/mm) spectrograph (Acton, Princeton Instruments, Inc., Trenton, NJ). An integration time of 0.3 s was used to collect each spectrum. The baseline correction was performed with WiTec Project 2.10 software (Witec GmbH, Germany) using a fifth order polynomial. Further smoothing to the spectra was performed using OriginPro 9.0.0 (OriginLab Corporation, Northampton, MA). Raman images were constructed by integrating characteristic bands presented in **Table 2**.

Table 2. Raman bands of cell wall polymers used to construct images[96]

Polymers	Raman bands (cm^{-1})	Raman modes
Lignin	1583-1620	Aromatic ring
Cellulose	1120-1130	C-O stretch

In this investigation, 14 regions of interest (ROI) from unextracted and extracted sections were scanned (**Figure 14**). Images of the intensity ratio between lignin and cellulose bands in the ROIs were produced. The ratio images provide reliable chemical information because artefacts caused by the surface unevenness and changes in the laser intensity are greatly reduced.[66] Average Raman spectra were produced by drawing ROIs in the S_2 layer and compound middle lamella (also cell corner middle lamellae) of the cell wall using WiTec Project software to monitor lignin extraction. Since there was severe section removal during the extraction, mapping the same ROI before and after the extraction could not be performed.

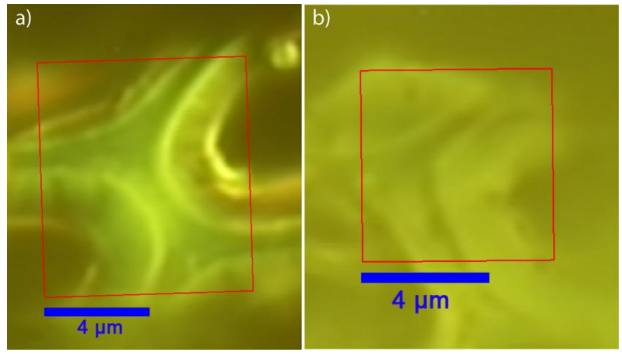

Figure 14. Original ROIs where mapping was performed before (a) and after (b) the extraction.

4. Results and Discussions

4.1 Cellulose elementary fibril orientation

Transmission electron microscopy (TEM) was performed on ultrathin spruce wood sections to investigate the cellulose elementary fibril (EF) orientation in different cell wall layers. Both two- (2D) and three-dimensional (3D) imaging techniques within TEM were used to obtain high-resolution information on the EF orientation.

4.1.1 Out-of-plane fibril angle in the secondary wall

It was believed that the wood cells have EFs that are helically oriented in the concentric plane of wood cell wall. A majority of the techniques employed to detect the EF angle in the wood cell wall report only the angle with respect to the longitudinal axis.[48] However, in this study, we found that EFs form an out-of-plane angle with respect to the tangential cell wall plane (**Figure 15**). This points out that there are at least two important angles in the cell wall: first one is the EF angle with respect to the longitudinal axis *i.e.*, microfibril angle (MFA)[48] and the second is the out-of-plane angle with respect to the concentric/tangential cell wall plane. An out-of-plane fibril angle was observed in all the layers of the secondary wall and is discussed in the following chapters.

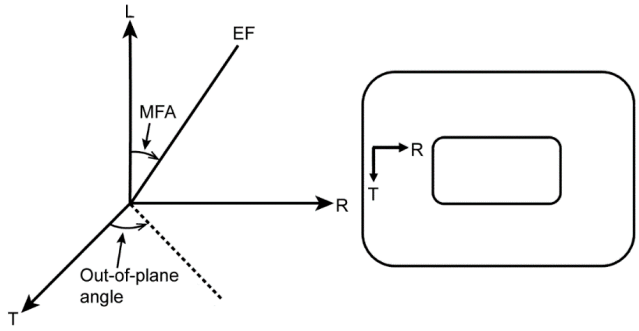

Figure 15. Conceptual diagram of out-of-plane angle, the fibril angle with respect to the concentric/tangential cell wall plane; EF, elementary fibril; MFA, microfibril angle, a frequently used acronym to denote fibril angle with respect to the longitudinal axis; L, longitudinal axis; R, radial axis; T, tangential axis.

4.1.2 Elementary fibril structures

Tomographic volumes show that the EFs in the secondary wall aggregate into bundles of different sizes (**Figure 16**). The size of the smaller aggregates *i.e.*,

EF bundles (EFB) was in the range of 30 - 50 nm. EFs in the EFBs seem to be bridged frequently (**Figure 16d**). Bridging of EFs by interfibrillar-bridging elements was observed in pulp and holocellulose.[31] The bridging can be served by hemicelluloses as this component is only slightly stained by $KMnO_4$ giving an almost similar electron density of cellulose in the tomograms.[80] Therefore, a mantle of hemicelluloses may be present at the periphery of the EFs.[110] The presence of EFBs of varying sizes in the tracheid S_2 layer was reported in several studies.[6,8,9] Xu and colleagues[9] presented a 3D model of an EFB with associated matrix materials based on the electron tomography of the lignin extracted S_2 layer. A positive correlation between the size of EF structure and degree of lignification was reported in a previous study.[10] When a tomographic subvolume containing an EFB was fitted with parametric space curves, it revealed the nanoscale geometries of EFs in an EFB. A tight arrangement of EFs can be seen in an EFB obtained from the S_1 layer (**Figure 16e**). The observed nanoscale geometries of the EFs can perhaps be described as curved, bundled and not straight over the length scales used here, which is consistent with previous studies.[9,76] In some regions, such as that presented in **Figure 16e**, helical bundles of EFs were observed.

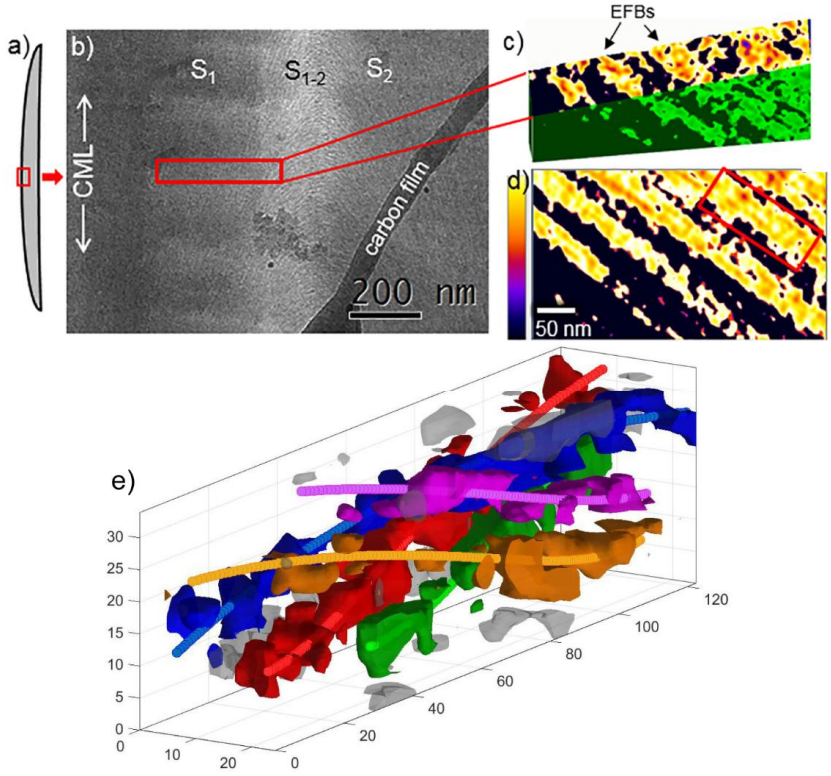

Figure 16. TEM tomography of S_1 layer. (a) A cartoon of a tracheid; (b) micrograph of a radial longitudinal section at 0° tilt; (c) 3D tomogram of a series of EFBs; (d) same tomogram with a transverse view (~90° vertical rotation of image c), the colour bar shows the tomographic density; and (e) parametric space curves fitted to a subvolume (red box in image d) containing a EF bundle, the plot unit is nm (Publication 3).

4.1.3 S_1 layer

Figure 17 shows that EFs in the S_1 layer have a large longitudinal EF angle and, simultaneously, a tilt relative to the cell wall plane (**Figure 15**). No sign of alternate S- and Z-helices in the S_1 layer was observed, corresponding to a study made by Brändström *et al.*[49] on Norway spruce, who observed more or less perpendicular EF orientation with respect to the longitudinal axis. A predominant radial lamellar organization of S_1 EFs is visible in a tomographic slice of radial longitudinal section (**Figure 17c**). Basically, the fibrillar texture visible in the 2D TEM images of S_1 longitudinal sections originates from the radial arrangement of EFBs (**Figure 17b,d**), where only the cross sections of the EFs and the EFBs are visible. The width of the S_1 layer was in the range of 200 – 600 nm. According to the literature, the S_1 layer of the secondary wall has transversely oriented EFs with an S-helical organization,[14,17,21,47,49-51] which is supported by the findings of this study. However, a crossed-fibrillar structure with super-imposed grid system was also reported in early studies.[20,52]

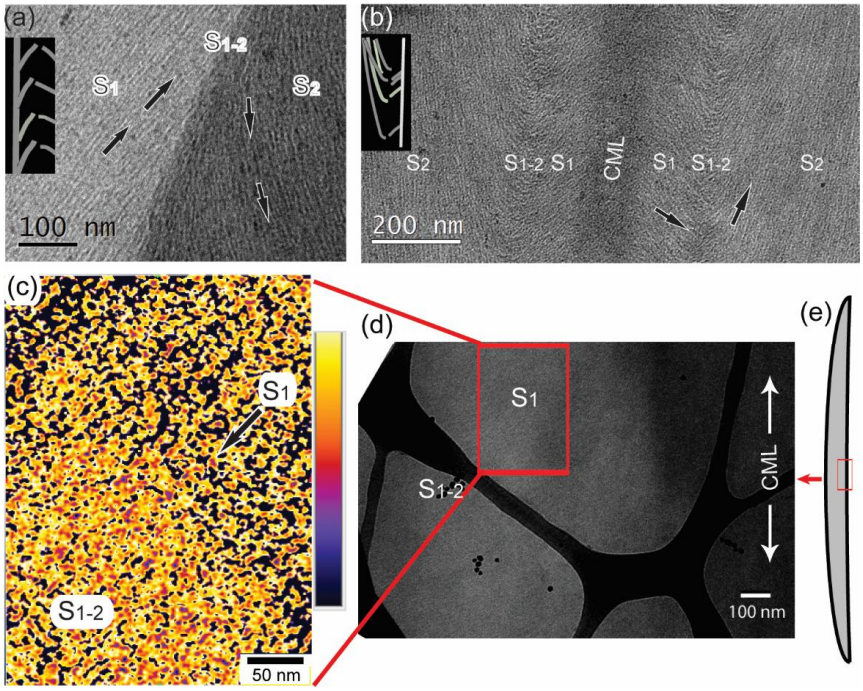

Figure 17. Micrographs of the wood sections showing EF orientation in different layers: (a) S_1, S_2 and S_{1-2} transition layer taken from cell corner region of a latewood tracheid with a part of the cell wall model (inset), an out-of-plane EF orientation is present in the S_1 and outer-S_2 layer, arrows show the EF orientation; (b) TEM image of the radial longitudinal section of the earlywood. A small part of the cell wall model is inserted for comparison. A radial fibrillar texture is apparent in the S_1 layer (arrow) and an out-of-plane EF orientation is visible in the outer-S_2 layer (arrow); (c) a tomographic slice of the S_1 layer showing the radially organized (arrow) lamellae, the colour bar shows the tomographic density; (d) TEM image of a radial longitudinal section at 0° tilt; and (e) a diagram of tracheid showing the location of tomography. CML, compound middle lamellae (Publications 2 and 3)

4.1.4 $S_{1\text{-}2}$ layer

The $S_{1\text{-}2}$ transition layer in the 2D electron micrographs can be recognized by the drastic change of EF angle (**Figure 17a,b**). The tomographic slices show that both parallel (**Figure 18**) and crossed-fibrillar (**Figure 19**) structures exist in this layer. The latter, however, gives a denser structure in the $S_{1\text{-}2}$ layer (**Figure 19**). The crossed-fibrillar structure in the $S_{1\text{-}2}$ layer suggests the presence of a dramatic change of helices from S-helix in the S_1 layer to Z-helix in the S_2 layer. Furthermore, the crossed-fibrillar structure in the $S_{1\text{-}2}$ layer is possible when out-of-plane EF orientations in the S_1 and outer-S_2 layer exist. The 3D tomographic volumes also show that the EFB lamellae intersect in the transition layer and are visible in the longitudinal sections (**Figure 18a**). When a tomographic subvolume extracted from a $S_{1\text{-}2}$ layer tomogram was fitted with parametric space curves, it revealed the crossed fibrillar structure with enhanced resolution (**Figure 19c**). Several studies demonstrated that the transition between S_1 and S_2 layers form a weak zone, where the defibration mainly takes place in mechanically stressed wood, indicating a dramatic change of EF orientation between these two layers.[49,111,112] The parallel EF orientation in the $S_{1\text{-}2}$ layer, on the other hand, suggests a gradual change of helices from S_1 to S_2. This observation is supported by a high-resolution SEM study on developing tracheids.[113] It should also be noted that the fibril angle in developing cell walls continuously changes until the cessation of cell expansion.[29]

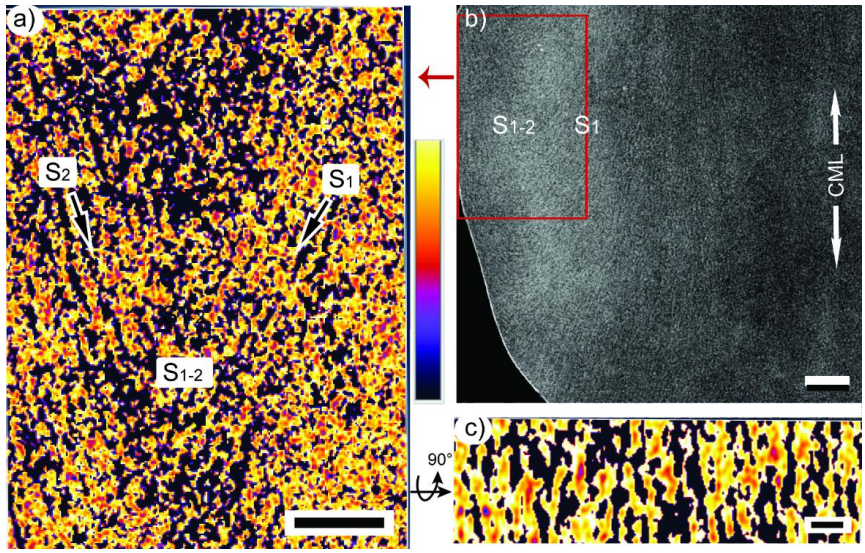

Figure 18. Tomography of the $S_{1\text{-}2}$ layer. (a) Tomographic slice of a longitudinal section shows that EF lamellae approaching from S_1 and S_2 layer cross (arrow) in the $S_{1\text{-}2}$ transition layer, the colour bar shows the tomographic density; (b) TEM image of a radial longitudinal section at 0° tilt; and (c) a 90° vertical rotation of image *a* shows a parallel EF orientation in the $S_{1\text{-}2}$ transverse section; all scale bars are 50 nm. (Publication 3).

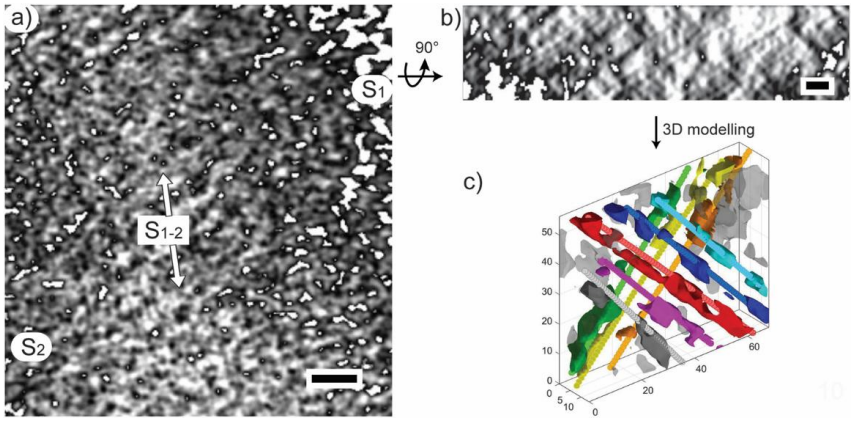

Figure 19. 3D tomography of the S_{1-2} longitudinal section. (a) A tomographic slice of the S_{1-2} layer shows a dense region (arrow); (b) a cross-fibrillar structure can be seen in the transverse section (90° vertical rotation of image *a*); all scale bars are 50 nm; (c) 3D modelling shows a crossed fibrillar structure in the S_{1-2} layer, the plot unit is nm (Publication 3).

4.1.5 S_2 layer

The micrographs of the longitudinal (tangential and radial) sections show that EFs in the outer-S_2 layer (next to the S_{1-2}) form a relatively large out-of-plane angle which continues to drop inward and becomes almost axial in the inner-S_2 layer (**Figures 17b and 20a**). The image of the outer-S_2 layer presented in **Figure 17a** shows the partially out-of-plane orientation of EFs in the transverse section, too. An axial EF angle in the inner-S_2 was also observed with Raman microscopy.[95] A Z-helical orientation in the S_2 layer was frequently reported in the previous studies.[17,21,48,49,51] An abrupt change in the EF orientation between S_2 and S_3 layers can be seen in the secondary wall transverse section (**Figure 20b**).

4.1.6 S_3 layer

A transverse out-of-plane EF orientation in the transverse sections of the S_3 layer was observed (**Figure 20b**). However, in the longitudinal sections (both radial and tangential), the S_3 layer seemed to have an EF orientation that was difficult to differentiate from the inner-S_2 layer of the same cell wall (**Figure 20a**). Transverse EF orientation with an S-helical organization in the S_3 layer was reported in several studies.[17,21,47,48,51] It should also be noted that the orientation of EFs in this layer varies considerably depending on the stage of deposition and position in the growth rings.[51,114]

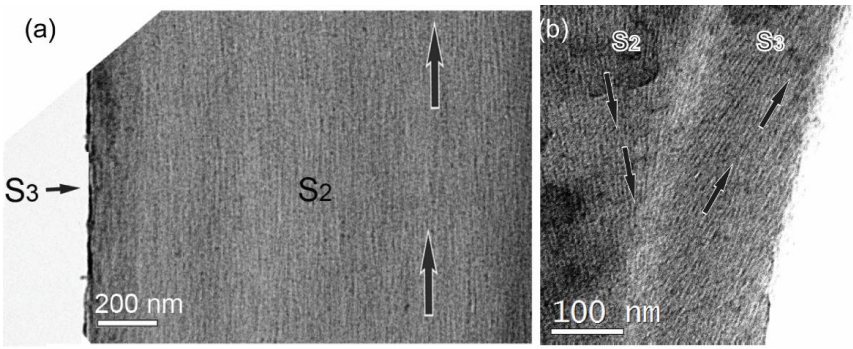

Figure 20. TEM image of longitudinal (a) and transverse (b) sections. (a) Micrograph of a tangential longitudinal section showing the axial EF orientation in the inner-S_2; and (b) image of the S_2 and S_3 layers taken from the cell corner region of a latewood tracheid where an abrupt change in EF orientation is apparent between the layers, and an out-of-plane EF orientation is visible in the S_3 layer (Publication 2).

4.2 Cell wall structure of thermomechanical pulps

The ultrathin transverse sections of thermomechanical pulp (TMP) fibers were studied with TEM. Micrographs showed that the defibration in TMPs refined at 130 °C and 150 °C predominantly takes place between the S_1 and S_2 layers (**Figure 21**). Fibrillation in the S_1 and outer-S_2 layer was also observed at 130 °C (**Figure 21a**). However, TMPs refined at 170 °C occasionally had exposed middle lamella on the pulp surface. TEM investigation of the native wood cell wall presented in this study showed a dramatic change of EF angle between the S_1 and S_2 layers (**Figure 17**) that likely contributes to the structural weakness in the $S_{1\text{-}2}$ transition zone. This observation is supported by several previous works.[49,70] Nevertheless, the defibration mechanism in the TMP fibers may vary depending on the concentration and chemical composition of lignin in native wood.[66,89]

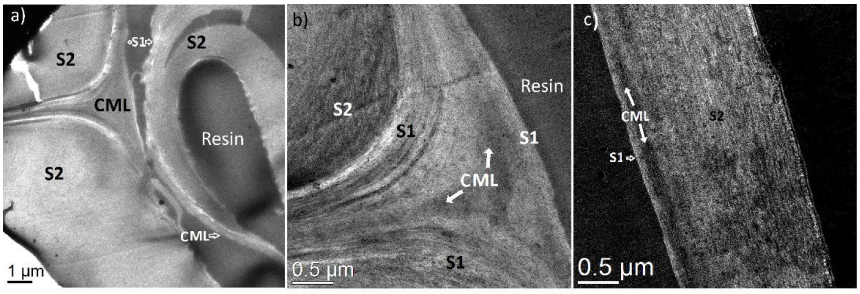

Figure 21. Transmission electron micrographs of TMP fiber transverse sections refined at 130 °C (a) and 150 °C (b, c). These images show that the defibration mainly takes place between the S_1 and S_2 layers at elevated temperature (Publication 4).

4.3 Wood cell wall model

Based on the results obtained with TEM, models of the wood cell wall are presented in **Figure 22** where, in contrast to the existing understanding, EFs

protrude from the concentric cell wall plane towards the lumen by forming an out-of-plane angle (arrows in **Figure 22b**). The expanded model of the S_1 layer (**Figure 22c**) shows that the transversely oriented EFBs (white) consisting of EFs embedded in the matrix (violet), form an out-of-plane angle in the transverse section and organize into radial lamellae in the longitudinal sections. However, the angle of the radial arrangement of lamellae can vary from cell to cell. Based on different assessment techniques, several models of the wood cell wall have been developed describing the average orientation of cell wall materials in different layers where an S–Z–S helical organization in the S_1, S_2, and S_3 layers can be seen, respectively.[21,23,47,52] Kerr and Goring[4] proposed a model of the S_2 layer depicting the average distribution of matrix materials and the arrangement of EFs in the lamellae. A modification to the individual fibril alignment in their model was suggested by Donaldson[115], based on computer modelling. Based on SEM, a modification to the Côté's[23] model was published by Sell and Zimmermann[11]. They added radial fibril agglomerations in the S_2 layer, which were again disputed by a study made by Fahlén and Salmén[7]. Some of the models developed in the 1950s depicted the crossed-fibrillar structure in the S_1 layer,[20,52] which was not supported by many subsequent studies. Another area of disagreement has been the arrangement of the lamellar structure in the S_2 layer, a discussion of whether it is radial or tangential.[7,11,54]

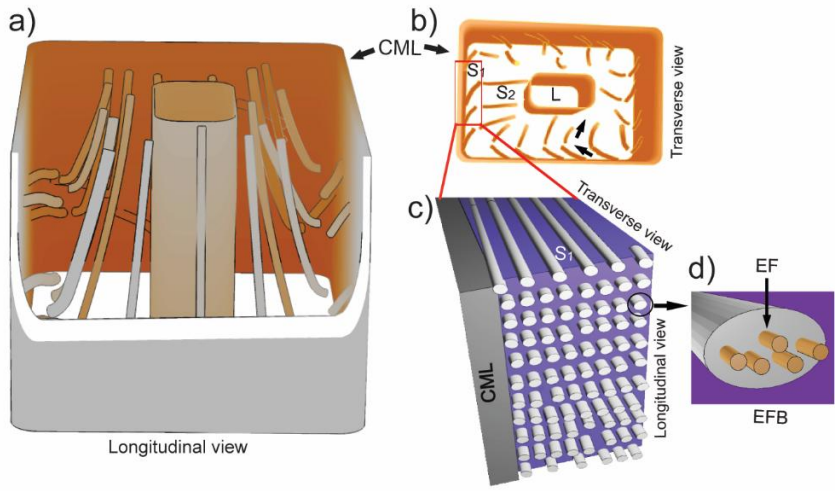

Figure 22. Cell wall models: (a, b) models of whole cell with average fibril (EF) orientation. Protruding EFs form an out-plane angle (arrows in b) with respect to the concentric cell wall plane; (c) a comprehensive model of the S_1 layer. A predominantly radial lamellar organization of EF bundles (EFB) is depicted; and (d) an EFB consisting of EFs. L, lumen; CML, compound middle lamellae (Publications 2 and 3).

4.4 Distribution of residual lignin in solvent extracted sections

Both Raman microspectroscopy and Transmission Electron Microscopy (TEM) were used to analyse ultrathin sections of spruce branch wood to trace the progress of lignin extraction with 1,4-dioxane. Average Raman spectra

from the S_2 layer and compound middle lamella (CML) from unextracted and extracted sections are shown in **Figure 23**; lignin and cellulose had the most prominent bands and can be easily distinguished. The spectral features of the extracted lignin from the CML and S_2 layer were also obtained by subtracting extracted spectra from an unextracted one (**Figure 23c,d**). Before subtraction, both spectra were normalized at the 1122 cm^{-1} cellulose band. In this way, it was estimated that ~ 39 % of the S_2 lignin was extracted. Similar normalization could not be applied to the CML spectra because of the lack of carbohydrate peaks in the spectra. Alternatively, the intensity ratio of the lignin band in the CML and S_2 layer (I_{CML}:I_{S2}) before and after the extraction were determined. As the imaging conditions of each sample were unchanged and it was known that $I_{extracted\text{-}S2} = 0.61 \times I_{unextracted\text{-}S2}$, the estimated fraction of the CML lignin extracted was ~ 46 %.

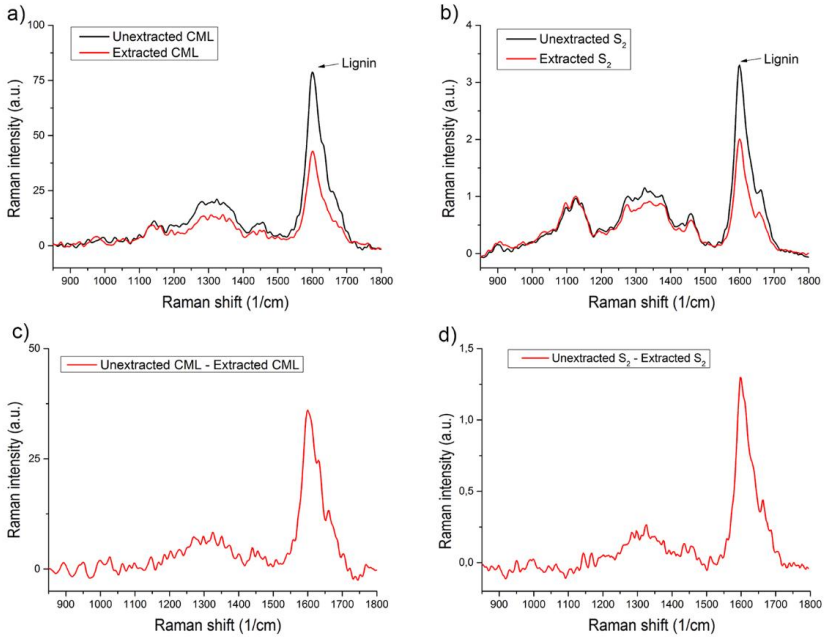

Figure 23. Raman spectra of unextracted and extracted sections. (a, b) Spectra of CML and S_2 layer before and after the extraction, respectively; and (c, d) subtracted spectra of CML and S_2 layer, respectively (Publication 5).

Raman images constructed according to the intensity ratio I_{1600}/I_{1122} before and after 1 h of extraction are presented in **Figure 24**; substantial changes in the chemical composition of the CML and the secondary wall can be seen in association with a reduction in scattering intensity from the lignin derived band at 1600 cm^{-1} (**Figure 23**). High lignin content can be seen only in the cell corner middle lamellae (CCML) after extraction.

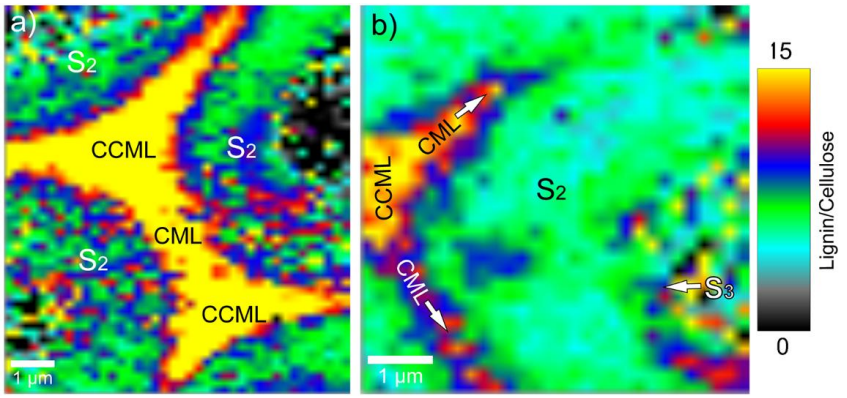

Figure 24. Lignin-cellulose ratio images of unextracted (a) and extracted (b) sections constructed with characterstic lignin and cellulose Raman bands. Unextracted CML shows the highest intensity that becomes narrower upon extraction. A significant change of colour intensity is also visible in the secondary wall. CCML, cell corner middle lamellae; CML, compound middle lamellae (Publication 5).

The $KMnO_4$ stained wood sections (both extracted and unextracted) were analysed with TEM. The different cell wall layers showed notable contrast differences depending on the concentration of lignin. Micrographs of the unextracted sections showed a heavily stained CML with an almost even staining of the other areas of the cell wall (**Figure 25a**); whereas, an intense staining was observed in the CML, cell corners (CCML), and S_3 layer of the extracted sample (**Figure 25b**). The S_2 layer of extracted cell wall was clearly less stained with $KMnO_4$. The CML with dark contrast also became narrower after extraction. These results correspond to an earlier study made by Maurer and Fengel who studied the sources of milled wood lignin using TEM.[116]

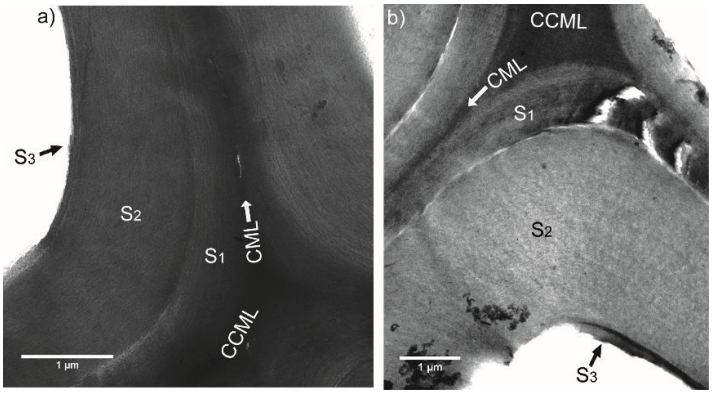

Figure 25. Transmission electron micrographs of unextracted (a) and extracted (b) sections. A gradient of lignin distribution between CML and the secondary wall can be seen in the unextracted sample, whereas a sharp difference in lignin distribution is present in the extracted one. Crack like features appeared in the extracted S_1 layer. CCML, cell corner middle lamellae; CML, compound middle lamellae (Publication 5).

This study clearly showed that 1,4-dioxane can partly extract lignin not only from the middle lamella but also from the secondary wall, although the wood section is much thicker (~ 200 nm) than the dimensions of elementary fibrils

(~ 3.5 nm). This is an unanticipated observation as the cell wall is generally considered as a tightly packed composite from which the matrix (lignin and hemicellulose) material is physically difficult to remove. Moreover, lignin and hemicelluloses are partly associated with each other through covalent linkages forming lignin–carbohydrate complexes.[117] For comparison, it is known that a fraction of the cell wall polysaccharides is solubilized during mechanical pulping of wood.[118] However, it is not possible to extract a large amount of lignin–hemicellulose complexes because 1,4-dioxane is not a solvent for hemicellulose and also our samples were not mechanically pre-processed. There are, however, many factors that govern the extent of extraction with 1,4-dioxane, such as the amount of possible lignin–hemicellulose bonds.

5. Conclusions

This thesis presents the structure and organization of cellulose elementary fibrils (EF) in tracheid walls using transmission electron microscopy (TEM) and image analysis. Two-dimensional (2D) electron micrographs and three-dimensional (3D) tomographic volumes reconstructed from the tilt series showed the detailed structure of S_1, S_{1-2}, S_2, and S_3 layers. It is apparent from the observations presented that several levels of complexity exist in the ultrastructure of the wood cell wall. The organization of EFs varies from layer to layer and also within a single layer. In addition to the well-adopted concept of varying longitudinal EF angle between the layers, these results point out the importance of the out-of-plane orientation of EFs relative to the cell wall plane. Therefore, the results differ from the prevailing model of concentric, planar lamella of helically organized EFs. The models of the wood cell wall based on 2D and 3D imaging techniques summarize most of the findings regarding the wood ultrastructure.

A predominant transverse EF orientation was present in the S_1 layer. Furthermore, EFs protruded from the concentric cell wall plane towards the lumen in an out-of-plane angle. The presence of EF aggregates in the form of bundles (EFB) of varying sizes was observed in the tomographic volumes of the S_1 layer. These EFBs organized into radially oriented lamellae in the S_1 longitudinal sections. Both crossed and parallel EF orientations were detected in the S_{1-2} transition layer. The presence of a distinctive EF orientation in the S_{1-2} layer is supported by the defibration mechanisms in the thermomechanical pulps (TMP). The defibration mainly took place between the S_1 and S_2 layer in TMPs. EFs in the outer-S_2 layer of wood specimens had a relatively high fibril angle with respect to the longitudinal axis and a large out-of-plane angle with respect to the tangential/concentric cell wall plane, which continued to decline inward and became almost axial in the inner-S_2 layer. A transverse, out-of-plane EF orientation in the transverse sections of the S_3 layer was observed. However, in longitudinal sections the S_3 layer seemed to have an EF orientation that was difficult to distinguish from the inner-S_2 layer.

Fitting the parametric space curves to the tomographic subvolumes showed the nanoscale geometries of the individual EFs in the S_1 and S_{1-2} layer. Qualitatively, the EF geometries can perhaps be described as curved, bundled and not straight.

The study of the lignin-extracted ultrathin sections provided valuable information regarding the cell wall behaviour during extraction when all the layers are exposed to solvent. The concentration of lignin in all cell wall layers

changed during the extraction process. However, lignin obtained after extraction consists mainly of secondary wall lignin as this area contains most of the total cell wall lignin in conifer tracheids. The presence of crack-like damage in the S_1 layer of the secondary wall was observed after extraction. Both Raman and TEM produced similar results.

5.1 Limitations and outlook

The results presented in this thesis were obtained mainly with transmission electron microscopy by analysing ultrathin wood sections. A problem with the very high magnification is that it is sometimes difficult to see where exactly the images were taken from. To overcome this issue, a low-magnification image covering the major parts of the cell wall was taken before going for a high-magnification image of a particular location. The ultrathin sections of wood microtomed from radial and tangential longitudinal planes were assumed to predominantly contain tangential and radial walls respectively. However, deviations from this anticipation could happen due to the high variability in the cell wall geometry.[14] Micrographs of the tangential sections of the tangential wall, and the radial sections of the radial wall are equally important to obtain detailed information of the cell wall. This difficulty was, however, significantly overcomed by electron tomography, which gives three-dimensional information of the wood cell wall. The cell wall model does not represent primary wall and S_3 layer which could not be imaged effectively because of small width.

In the lignin extraction paper, the accessibility of lignin by 1,4-dioxane in ultrathin sections was mainly focused, and therefore, the outcomes could be different in the case of thicker specimens.

The wood material in this study was limited to Norway spruce free of abnormalities, such as knots. Further study on different wood species would be needed to observe the possible deviations from the model presented in this study. The behavior of wood under stress could also be tested with regard to the proposed model of wood cell wall.

The presented model has some details of the wood cell wall structures that have been overlooked for decades. The addition of the out-of-plane concept would assist researchers to unravel many of the challenges regarding the behavior of wood under mechanical stress as well as the biosynthesis of cellulose elementary fibrils in the developing cell wall. Research on the mechanisms of cell wall expansion in connection with the proposed model would provide valuable information on developing cell wall. Furthermore, the introduction of the out-of-plane angle in the model will help to understand the formation of radial/tangential patterns by elementary fibril structures in the secondary wall. An additional methods could, however, be applied to confirm the data on out-of-plane fibril angle. There are many additional findings that could not be included in the model, but will have important role in future research. The new observations on the orientation of EFs may also lead to a better understanding of the reactivity of cellulosic fibers in biochemical, chemical and mechanical treatments.

References

1. Frey-Wyssling, A. The ultrastructure of wood. *Wood Sci. Technol.* 1968, 2, 73-83.
2. Preston, R. D. *The physical biology of plant walls;* Chapman & Hill: London, 1974, pp 491.
3. Daniel, G. In *Wood and fiber morphology;* Ek, M., Gellerstedt, G. and Henriksson, G., Eds.; Ljungberg textbook: Pulp and paper chemistry and technology; Fiber and Polymer Technology, KTH: Stockholm, 2007; pp 49-71.
4. Kerr, A. J.; Goring, D. A. I. Ultrastructural arrangement of the wood cell wall. *Cellulose Chem. Technol.* **1975***, 9*, 563-573.
5. Ponni, R.; Vuorinen, T.; Kontturi, E. Proposed Nano-Scale Coalescence of Cellulose in Chemical Pulp Fibers during Technical Treatments. *BioResources* **2012***, 7*, 6077-6108.
6. Singh, A. P.; Daniel, G. The S2 layer in the tracheid walls of *Picea abies* wood: inhomogeneity in lignin distribution and cell wall microstructure. *Holzforschung* **2001***, 55*, 373-378.
7. Fahlén, J.; Salmén, L. On the lamellar structure of the tracheid cell wall. *Plant Biol.* **2002***, 4*, 339-345.
8. Singh, A.; Daniel, G.; Nilsson, H. Ultrastructure of the S2 layer in relation to lignin distribution in *Pinus radiata* tracheids. *J. Wood Sci.* **2002***, 48*, 95-98.
9. Xu, P.; Donaldson, L. A.; Gergely, Z. R.; Staehelin, L. A. Dual-axis electron tomography: a new approach for investigating the spatial organization of wood cellulose microfibrils. *Wood Sci. Technol.* **2007***, 41*, 101-116.
10. Donaldson, L. A. Cellulose microfibril aggregates and their size variation with cell wall type. *Wood Sci. Technol.* **2007***, 41*, 443-460.
11. Sell, J.; Zimmermann, T. Radial fibril agglomerations of the S2 on transverse-fracture surfaces of tracheids of tension-loaded spruce and white fir. *Holz Roh-Werkst* **1993***, 51*, 384.
12. Bucur, V. Techniques for high resolution imaging of wood structure: a review. *Meas. Sci. Technol.* **2003***, 14*, R91-R98.
13. Lachaud, S.; Catesson, A. M.; Bonnemein, J. L. Structure and functions of the vascular cambium (review). *C. R. Acad. Sci. III.* **1999***, 322*, 633-650.
14. Brändstrom, J. Micro- and ultrastructural aspects of Norway spruce tracheids: A Review. *IAWA J.* **2001***, 22*, 333-353.
15. Sjöström, E. *Wood Chemistry: Fundamentals and Applications;* Academic Press Inc.: San Diego, CA, USA, 1993, pp 293.
16. Eder, M.; Arnould, O.; Dunlop, J. W. C.; Hornatowska, J.; Salmén, L. Experimental micromechanical characterisationof wood cell walls. *Wood. Sci. Technol.* **2013***, 47*, 163-182.
17. Côté, W. A. Ultrastructure—Critical domain for wood behavior. *Wood Sci. Technol.* **1981***, 15*, 1-29.
18. Timell, T. E. Studies on opposite wood in conifers. Part III: Distribution of lignin. *Wood Sci. Technol.* **1973***, 7*, 163-172.
19. Singh, A.; Daniel, G.; Nilsson, T. High variability in the thickness of the S3 layer in *Pinus radiata* tracheids. *Holzforschung* **2002***, 56*, 111-116.
20. Wardrop, A. B. The Organization and Properties of the Outer Layer of the Secondary Wall in Conifer Tracheids. *Holzforschung* **1957***, 11*, 102-110.

21. Abe, H.; Funada, R. Review-The orientation of cellulose microfibrils in the cell walls of tracheids in conifers. *IAWA J.* **2005***, 26*, 161-174.
22. Prodhan, A. K. M. A.; Ohtani, J.; Funada, R.; Abe, H.; Fukazawa, K. Ultrastructural investigation of tension wood fiber in *Fraxinus mandshurica* Rupr. var. *Japonica Maxim*. *Ann. Bot.* **1995***, 75*, 311-317.
23. Côté, W. A. *Wood ultrastructure: an atlas of electron micrographs;* University of Washington Press: Seattle, Washington, 1967, pp 64.
24. Preston, R. D.; Nicolai, E.; Reed, R.; Millard, A. An electron microscope study of cellulose in the wall of *Valonia ventricosa*. *Nature* **1948***, 162*, 665-667.
25. Mühlethaler, K. Electron Micrographs of Plant Fibers. *Biochim. Biophys. Acta* **1949***, 3*, 15-25.
26. Mueller, S.; Brown, R. Evidence for an Intramembrane Component Associated with a Cellulose Microfibril-Synthesizing Complex in Higher-Plants. *J. Cell Biol.* **1980***, 84*, 315-326.
27. Emons, A. M.; Mulder, B. M. How the deposition of cellulose microfibrils builds cell wall architecture. *Trends Plant Sci.* **2000***, 5*, 35-40.
28. Paredez, A. R.; Somerville, C. R.; Ehrhardt, D. W. Visualization of cellulose synthase demonstrates functional association with microtubules. *Science* **2006***, 312*, 1491-1495.
29. Abe, H.; Funada, R.; Ohtani, J.; Fukazawa, K. Changes in the arrangement of microtubules and microfibrils in differentiating conifer tracheidsduring the expansion of cells. *Ann. Bot.* **1995***, 75*, 305-310.
30. Mühlethaler, K.; Muggli, R. Fine Structure of Cellulose Elementary Fibrils. *Papier* **1969***, 23*, 15.
31. Donaldson, L. A.; Singh, A. P. Bridge-like structure between cellulose microfibrils in radiata pine (*Pinus radiata* D.Don) kraft pulp and holocellulose. *Holzforschung* **1998***, 52*, 449-454.
32. Sugiyama, J.; Persson, J.; Chanzy, H. Combined infrared and electron diffraction study of the polymorphism of native celluloses. *Macromolecules* **1991***, 24*, 2461-2466.
33. Sugiyama, J.; Vuong, R.; Chanzy, H. Electron-Diffraction Study on the 2 Crystalline Phases Occurring in Native Cellulose from an Algal Cell-Wall. *Macromolecules* **1991***, 24*, 4168-4175.
34. Frey-Wyssling, V. A.; Mühlethaler, K. Die elementarfibrillen der cellulose. *Die Makromolekulare Chemie* **1963***, 62*, 25-30.
35. Fernandes, A. N.; Thomas, L. H.; Altaner, C. M.; Callow, P.; Forsyth, V. T.; Apperley, D. C.; Kennedy, C. J.; Jarvis, M. C. Nanostructure of cellulose microfibrils in spruce wood. *Proc. Natl. Acad. Sci.* **2011***, 108*, E1195-E1203.
36. Ding, S. Y.; Himmel, M. E. The maize primary cell wall microfibril: A new model derived from direct visualization. *J. Agric. Food Chem.* **2006***, 54*, 597-606.
37. Nishiyama, Y. Structure and properties of the cellulose microfibril. *J. Wood Sci.* **2009***, 55*, 241-249.
38. Nishiyama, Y.; Kim, U. J.; Kim, D. Y.; Katsumata, K. S.; May, R. P.; Langan, P. Periodic disorder along ramie cellulose microfibrils. *Biomacromolecules* **2003***, 4*, 1013-1017.
39. Adachi, H.; Sugiyama, J.; Kondo, Y.; Okano, T. The difference of cellulose crystal between softwoods and hardwoods. *Sen'i Gakkaishi* **1991***, 47*, 580-584.
40. Okita, Y.; Saito, T.; Isogai, A. Entire Surface Oxidation of Various Cellulose Microfibrils by TEMPO-Mediated Oxidation. *Biomacromolecules* **2010***, 11*, 1696-1700.
41. Hodge, A. J.; Wardrop, A. B. An electron-microscopic investigation of the cell-wall organisation of conifer tracheids. *Nature* **1950***, 165*, 272-273.

42. Manley, R. S. J. Fine Structure of Native Cellulose Microfibrils. *Nature* **1964***, 204*, 1155-1157.
43. Hult, E. L.; Larsson, P. T.; Iversen, T. Cellulose aggregation—an inherent property of Kraft pulps. *Polymer* **2001***, 42*, 3309-3314.
44. Reza, M.; Ruokolainen, J.; Vuorinen, T. Out-of-plane orientation of cellulose elementary fibrils on spruce tracheid wall based on imaging with high-resolution transmission electron microscopy. *Planta* **2014***, 240*, 565-573.
45. Singh, A.; Sell, J.; Schmitt, U.; Zimmermann, T.; Dawson, B. Radial striation of the S2 layer in mild compression wood tracheids of *Pinus radiata*. *Holzforschung* **1998***, 52*, 563-566.
46. Krässig, H. A. *Cellulose - Structure, Accessibility and Reactivity;* Gordon and Breach Science Publishers: Yverdon, Switzerland, 1993.
47. Wardrop, A. B. The fine structure of the conifer tracheid. *Holzforschung* **1954***, 8*, 12-29.
48. Donaldson, L. Microfibril angle: measurement, variation and relationships—a review. *IAWA J.* **2008***, 29*, 345-386.
49. Brändström, J.; Bardage, S. L.; Daniel, G.; Nilsson, H. The structural organization of the S1 cell wall layer of Norway spruce tracheids. *IAWA J.* **2003***, 24*, 27-40.
50. Donaldson, L.; Xu, P. Microfibril orientation across the secondary cell wall of Radiata pine tracheids. *Trees* **2005***, 19*, 644-653.
51. Abe, H.; Ohtani, J.; Fukazawa, K. Microfibrillar orientation of the innermost surface of conlfer tracheid walls. *IAWA Bull n. s.* **1992***, 13*, 411-438.
52. Emerton, H. W.; Goldsmith, V. The Structure of the Outer Secondary Wall of Pine Tracheids from Kraft Pulps. *Holzforschung* **1956***, 10*, 108-115.
53. Maurer, A.; Fengel, D. Elektronenmikroskopische Darstellung von strukturellen Einzelheiten in Nadelholz-Zellwänden anhand sehr dünner Ultramikrotomschnitte. *Holz Roh- Werkst* **1991***, 49*, 53-56.
54. Chafe, S. C. On the lamellate structure of the S2 layer. *Protoplasma* **1974***, 79*, 745-158.
55. Fengel, D.; Wegener, G. *Wood: Chemistry, Ultrastructure, Reactions;* Walter de Gruyter: Berlin, 1984, pp 513.
56. Wardrop, A. B. In *The structure and formation of the cell wall in xylem;* Zimmermann, M. H., Ed.; *The formation of wood in forest trees*; Academic Press, New York: 1964.
57. Abe, H.; Ohtani, J.; Fukazawa, K. FE-SEM observations on the microfibrillar orientation in the secondary wall of tracheids. *IAWA J.* **1991***, 12*, 431-438.
58. Ma, J.; Zhang, Z.; Yang, G.; Mao, J.; Xu, F. Ultrastructural topochemistry of cell wall polymers in *Populus nigra* by transmission electron microscopy and Raman imaging. *BioResources* **2011***, 6*, 3944-3959.
59. Dixon, R. A.; Chen, F.; Guo, D. and Parvathi, K. The biosynthesis of monolignols: a "metabolic grid", or independent pathways to guaiacyl and syringyl units? *Phytochemistry* **2001***, 57*, 1069-1084.
60. Henriksson, G. In *Lignin;* Ek, M., Gellerstedt, G. and Henriksson, G., Eds.; Ljungberg textbook: pulp and paper technology; Fiber and Polymer Technology, KTH: Stockholm, 2007; Vol. 1, pp 125-148.
61. Hafrén, J.; Fujino, T.; Itoh, T.; Westermark, U.; Terashima, N. Ultrastructural Changes in the Compound Middle Lamella of *Pinus thunbergii* During Lignification and Lignin Removal. *Holzforschung* **2000***, 54*, 234-240.
62. Kim, Y. S.; Lee, K. H.; Kim, J. S.; Singh, P. A. Lignin masks the presence of fibrillar network structure in the cell corner middle lamella (CCML). *Holzforschung* **2014***, 69*, 121-126.

63. Donaldson, L. A. Lignification and lignin topochemistry — an ultrastructural view. *Phytochemistry* **2001***, 57*, 859-873.
64. Fergus, B. J.; Procter, A. R.; Scott, A. N.; Goring, D. A. I. The distribution of lignin in sprucewood as determined by ultraviolet microscopy. *Wood Sci. Technol.* **1969***, 3*, 117-138.
65. Singh, A.; Kim, Y. S.; Chung, G. C.; Park, B. D.; Wong, A. H. H. TEM Examination of Surface Characteristics of Rubberwood (*Hevea brasiliensis*) HTMP Fibers. *Holzforschung* **2003***, 57*, 579-584.
66. Hänninen, T.; Kontturi, E.; Vuorinen, T. Distribution of lignin and its coniferyl alcohol and coniferyl aldehyde groups in *Picea abies* and *Pinus sylvestris* as observed by Raman imaging. *Phytochemistry* **2011***, 72*, 1889-1895.
67. Prislan, P.; Koch, G.; Čufar, K.; Gričar, J.; Schmitt, U. Topochemical investigations of cell walls in developing xylem of beech (*Fagus sylvatica* L.). *Holzforschung* **2009***, 63*, 482-490.
68. Fernando, D.; Muhic, D.; Engstrand, P.; Geoffrey, D. Fundamental understanding of pulp property development under different thermomechanical pulp refining conditions as observed by a new Simons' staining method and SEM observation of the ultrastructure of fibre surfaces. *Holzforschung* **2011***, 65*, 777-786.
69. Johansson, L.; Peng, F.; Simonson, R. Effects of temperature and sulfonation on shear deformation of spruce wood. *Wood Sci. Technol.* **1997***, 31*, 105-117.
70. Gustafsson, J.; Lehto, J. H.; Tienvieri, T.; Ciovica, L.; Peltonen, J. Surface characteristics of thermomechanical pulps; the influence of defibration temperature and refining. *Colloid Surf. A* **2003***, 225*, 95-104.
71. Williams, D. B.; Carter, C. B. *Transmission Electron Microscopy: A Textbook for Materials Science;* Springer: New York, 2009.
72. Reza, M., Kontturi, E., Jääskeläinen, A. -S., Vuorinen, T., Ruokolainen, J. Transmission Electron Microscopy for Wood and Fiber Analysis − A Review. *BioResources* **2015***, 10*, 6230-6261.
73. Sugiyama, J.; Otsuka, Y.; Murase, H.; Harada, H. Toward direct imaging of cellulose microfibrils in wood. *Holzforschung* **1986***, 40(Suppl.)*, 31-36.
74. Trtik, P.; Dual, J.; Keunecke, D.; Mannes, D.; Niemz, P.; Stähli, P.; Kaestner, A.; Groso, A.; Stampanoni, M. 3D imaging of microstructure of spruce wood. *J. Struct. Biol.* **2007***, 159*, 46-55.
75. Sali, A.; Glaeser, R.; Earnest, T.; Baumeister, W. From words to literature in structural proteomics. *Nature* **2003***, 422*, 216-225.
76. Ciesielski, P. N.; Matthews, J. F.; Tucker, M. P.; Beckham, G. T.; Crowley, M. F.; Himmel, M. E.; Donohoe, B. S. Microfibrils, 3D electron tomography of pretreated biomass informs atomic modeling of cellulose. *ACS Nano* **2013***, 7*, 8011-8019.
77. Bland, D. E.; Foster, R. C.; Logan, A. F. The mechanism of permanganate and osmium tetroxide fixation and the distribution of lignin in the cell wall of *Pinus radiata*. *Hozforschung* **1971***, 25*, 137-143.
78. Maurer, A.; Fengel, D. A New Process for Improving the Quality and Lignin Staining of Ultrathin Sections from Wood Tissue. *Holzforschung* **1990***, 44*, 453-460.
79. Blanchette, R. A.; Abad, A. R.; Cease, K. R.; Lovrien, R. E.; Leathers, T. D. Colloidal Gold Cytochemistry of Endo-1,4-beta-Glucanase, 1,4-beta-D-Glucan Cellobiohydrolase, and Endo-1,4-beta-Xylanase: Ultrastructure of Sound and Decayed Birch Wood. *Appl. Environ. Microbiol.* **1989***, 55*, 2293-2301.
80. Khristova, P.; Bentcheva, S.; Karar, I. Soda-AQ pulp blends from kenaf and sunflower stalks. *Bioresour. Technol.* **1998***, 66*, 99-103.

81. Koch, G.; Schmitt, U. In *Topochemical and Electron Microscopic Analyses on the Lignification of Individual Cell Wall Layers During Wood Formation and Secondary Changes;* Fromm, J., Ed.; Cellular aspects of wood formation; Springer-Verlag: Berlin Heidelberg, 2013; pp 41-69.
82. Lehringer, C.; Daniel, G.; Schmitt, U. TEM/FE-SEM studies on tension wood fibres of *Acer* spp., *Fagus sylvatica* L. and *Quercus robur* L. *Wood Sci. Technol.* **2009***, 43*, 691-702.
83. Donaldson, L. A. Abnormal lignin distribution in wood from severely drought stressed pinus radiata trees. *IAWA J.* **2002***, 23*, 161-178.
84. Donaldson, L. A. Ultrastructure of Transwall Fracture Surfaces in Radiata Pine Wood using Transmission Electron Microscopy and Digital Image Processing. *Holzforschung* **1997***, 51*, 303-308.
85. Bahr, G. F. Osmium tetroxide and ruthenium tetroxide and their reactions with biologically important substances: Electron stains III. *Exp. Cell Res.* **1954***, 7*, 457-479.
86. Hepler, P. K.; Newcomb, E. H. The Fine Structure of Young Tracheary Xylem Elements Arising by Redifferentiation of Parenchyma in Wounded Coleus Stem. *J. Exp. Bot.* **1963***, 14*, 496-503.
87. Saito, T.; Nishiyama, Y.; Putaux, J.; Vignon, M.; Isogai, A. Homogeneous Suspensions of Individualized Microfibrils from TEMPO-Catalyzed Oxidation of Native Cellulose. *Biomacromolecules* **2006***, 7*, 1687-1691.
88. Kallavus, U.; Gravitis, J. A Comparative Investigation of the Ultrastructure of Steam Exploded Wood with Light, Scanning and Transmission Electron Microscopy. *Holzforschung* **1995***, 49*, 182-188.
89. Fernando, D.; Daniel, G. Exploring Scots pine fibre development mechanisms during TMP processing: Impact of cell wall ultrastructure (morphological and topochemical) on negative behaviour. *Holzforschung* **2008***, 62*, 597-607.
90. Borgin, K.; Parameswaran, N.; Liese, W. The effect of aging on the ultrastructure of wood. *Wood Sci. Technol.* **1975***, 9*, 87-98.
91. Agarwal, U. P. Raman imaging to investigate ultrastructure and composition of plant cell walls: distribution of lignin and cellulose in black spruce wood (*Picea mariana*). *Planta* **2006***, 224*, 1141-1153.
92. Gierlinger, N.; Schwanninger, M. The potential of Raman microscopy and Raman imaging in plant research. *Plant physiol.* **2007***, 21*, 69-89.
93. Atalla, R. H.; Agarwal, U. P. Raman microprobe evidence for lignin orientation in the cell walls of native woody tissue. *Science* **1985***, 227*, 636-638.
94. Atalla, R. H.; Whitmore, R. E.; Heimbach, C. J. Raman spectral evidence for molecular-orientation in native cellulose fibres. *Macromolecules* **1980***, 13*, 1717-1719.
95. Gierlinger, N.; Luss, S.; König, C.; Konnerth, J.; Eder, M.; Fratzl, P. Cellulose microfibril orientation of *Picea abies* and its variability at the micron-level determined by Raman imaging. *J. Exp. Bot.* **2010***, 61*, 587-595.
96. Agarwal, U. P.; Ralph, S. A. FT-Raman spectroscopy of wood: Identifying contributions of lignin and carbohydrate polymers in the spectrum of black spruce (*Picea mariana*). *Appl. Spectrosc.* **1997***, 51*, 1648-1655.
97. Agarwal, U. P.; Ralph, S. A. Determination of ethylenic residues in wood and in TMP of spruce by FT-Raman spectroscop. *Holzforschung* **2008***, 62*, 667-675.
98. Nuopponen, M.; Willför, S.; Jääskeläinen, A. -S.; Sundberg, A.; Vuorinen, T. A UV resonance Raman (UVRR) spectroscopic study on the extractable compounds in Scots pine (*Pinus sylvestris*) wood. Part I: lipophilic compounds. *Spectrochim. Acta, Part A* **2004***, 60*, 2953-2961.

99. Nuopponen, M.; Willför, S.; Jääskeläinen, A. -S.; Vuorinen, T. A UV resonance Raman (UVRR) spectroscopic study on the extractable compounds in Scots pine wood (*Pinus sylvestris*). Part II: hydrophilic compounds. *Spectrochim. Acta, Part A* **2004***, 60*, 2963-2968.
100. Saariaho, A. -M.; Hortling, B.; Jääskeläinen, A. -S.; Tamminen, T.; Vuorinen, T. Simultaneous quantification of residual lignin and hexenuronic acid from chemical pulps with UV resonance Raman spectroscopy and multivariate calibration. *J. Pulp. Pap. Sci.* **2003***, 29*, 363-370.
101. Hänninen, T. Studies on the ultrastructure of natural fibres and its effects on the fibre utilization, Aalto University School of Chemical Technology, Helsinki, Finland, 2011.
102. Muguet, M. C. d. S.; Colodette, J. L.; Jääskeläinen, A. Alkaline peroxide mechanical pulping of novel Brazilian eucalyptus hybrids. *BioResources* **2012***, 7*, 3823-3836.
103. Mastronarde, D. N. Automated electron microscope tomography using robust prediction of specimen movements. *J. Struct. Biol.* **2005***, 152*, 36-51.
104. Kremer, J. R.; Mastronarde, D. N.; McIntosh, J. R. Computer Visualization of Three-Dimensional Image Data Using IMOD. *J. Struct. Biol.* **1996***, 116*, 71-76.
105. Schneider, C. A.; Rasband, W. S.; Eliceiri, K. W. NIH Image to ImageJ: 25 years of image analysis. *Nature Methods* **2012***, 9*, 671-675.
106. Pettersen, E. F.; Goddard, T. D.; Huang, C. C.; Couch, G. S.; Greenblatt, D. M.; Meng, E. C.; Ferrin, T. E. UCSF Chimera--a visualization system for exploratory research and analysis. *J. Comput. Chem.* **2004***, 25*, 1605-1612.
107. Zimmermann, T.; Thommen, V.; Reimann, P.; Hug, H. J. Ultrastructural appearance of embedded and polished wood cell walls as revealed by Atomic Force Microscopy. *J. Struct. Biol.* **2006***, 156*, 363-369.
108. Anonymous. *http://psotoolbox.sourceforge.net/* (Accessed October, 2015).
109. www.blender.org.
110. Salmén, L.; Burgert, I. Cell wall features with regard to mechanical performance. A review. *Holzforschung* **2009***, 63*, 121-129.
111. Solala, I.; Antikainen, T.; Reza, M.; Johansson, L.; Hughes, M.; Vuorinen, T. Spruce fiber properties after high-temperature thermomechanical pulping (HT-TMP). *Holzforschung* **2013***, 68*, 195-201.
112. Donaldson, L. A. Cell wall fracture properties in relation to lignin distribution and cell dimensions among three genetic groups of radiata pine. *Wood Sci. Technol.* **1995***, 29*, 51-63.
113. Abe, H.; Ohtani, J.; Fukazawa, K. FE-SEM observations on the microfibrillar orientation in the secondary wall of tracheids. *IAWA J.* **1991***, 12*, 431-438.
114. Paakkari, T.; Serimaa, R. A study of the structure of wood cells by x-ray diffraction. *Wood Sci. Technol.* **1984***, 18*, 79-85.
115. Donaldson, L. A. A three-dimensional computer model of the tracheid cell wall as a tool for inerpretations of wood cell wall ultrastructure. *IAWA J.* **2001***, 22*, 213-233.
116. Maurer, A.; Fengel, D. On the origin of milled wood lignin. *Holzforschung* **1992***, 46*, 471-475.
117. Albersheim, P.; Darvill, A.; Roberts, K.; Sederoff, R.; Staehelin, A. In *Principles of cell wall architecture and assemply;* Plant cell walls. From chemistry to biology; Garland Science: New York, USA, 2011; pp 227-272.
118. Thornton, J.; Ekman, R.; Holmbom, B.; Örså, F. Polysaccharides dissolved from Norway spruce in thermomechanical pulping and peroxide bleaching. *J. Wood Chem. Technol.* **1994***, 14*, 159-175.

Aalto-DD 39/2016

ISBN 978-952-60-6683-7 (printed)
ISBN 978-952-60-6684-4 (pdf)
ISSN-L 1799-4934
ISSN 1799-4934 (printed)
ISSN 1799-4942 (pdf)

Aalto University
School of Science
Department of Applied Physics
www.aalto.fi

BUSINESS +
ECONOMY

ART +
DESIGN +
ARCHITECTURE

SCIENCE +
TECHNOLOGY

CROSSOVER

DOCTORAL
DISSERTATIONS